NUMERICAL STUDY ON TRANSVERSE FRICTION OF A SLENDER ROD CONTACTING THE SEABED

A Thesis

by

HANG LU

Submitted to the Office of Graduate Studies of
Texas A&M University
in partial fulfillment of the requirements for the degree of

MASTER OF SCIENCE

August 2012

Major Subject: Ocean Engineering

Numerical Study on Transverse Friction of a Slender Rod Contacting the Seabed

NUMERICAL STUDY ON TRANSVERSE FRICTION OF A SLENDER ROD CONTACTING THE SEABED

A Thesis

by

HANG LU

Submitted to the Office of Graduate Studies of
Texas A&M University
in partial fulfillment of the requirements for the degree of

MASTER OF SCIENCE

Approved by:

Chair of Committee,	Jun Zhang
Committee Members,	Moo-Hyun Kim
	Ramesh Talreja
Head of Department,	John Niedzwecki

August 2012

Major Subject: Ocean Engineering

ABSTRACT

Numerical Study on Transverse Friction of a Slender Rod Contacting the Seabed.

(August 2012)

Hang Lu, B.S., Wuhan University of Technology

Chair of Advisory Committee: Dr. Jun Zhang

With the increasing developments of exploiting oil and natural gas in deep water and harnessing renewable (wave and wind) energy in the sea, mooring lines and risers are widely deployed to position the related floating structures. Subject to environmental loads, a mooring line or riser connected to floating structure, moves up and down, back and forth, and sometimes from the left to the right. In computation of the dynamics of a mooring line or riser, it is often modeled as a flexible slender rod. While the bending moment of a chain or a rope is neglected, that of a riser is considered and specified by characteristics of the riser. Existing numerical codes for simulating the dynamics of a slender rod, such as CABLE3D, allow for the vertical support force and longitudinal (along the direction of the rod) friction from soils of the seabed while the transverse (in the direction transverse to the slender rod) friction between the rod and the seabed soils is not considered. In this study, we extend the current version of CABLE3D to allow for the transverse friction applied on

the portion of a slender rod contacting the seabed soil, which is time-varying when it is moving. The friction between a slender rod and the seabed soil is computed based upon a Coulomb model originally developed for the simulation of the friction in all dry contact mechanical systems. In applying the Coulomb model, the transverse friction depends on the transverse displacement and/or velocity of a slender rod contacting the seabed. In addition, vertical bottom support of the seabed soil is calculated based on the shear stress of the seabed soil. The simulations of the dynamics of a few typical mooring lines are made given their motions at their fairleads and the results are compared with the corresponding results obtained using Orcaflex, a commercial code, and the existing version of CABLE3D.

ACKNOWLEDGEMENTS

First and foremost, I would like to thank my committee chair, Dr. Jun Zhang, for his utmost supervision in the process of the research. This thesis would not have been possible without his guidance and help. He showed me exactly what it takes to be a responsible researcher. Also, thanks so much to my committee members, Dr. Kim and Dr. Talreja, for their kindly assistance and attention. Last but not least, I owe my gratitude to my colleagues and the department faculty and staff for making my time at Texas A&M University a wonderful experience.

TABLE OF CONTENTS

LIST OF FIGURES

Page

LIST OF TABLES

Page

1. INTRODUCTION

1. 1 Background and significance

As exploitation of ocean energy increases, especially in ever deeper water, more and more attention has been drawn to dynamic behavior of mooring lines and risers, which were proven to be of significance for analysis of global performance of floating platform (Nakamura et al., 1991).

In analyzing a mooring system, mooring lines are generally classified based on their geometry characteristic: taut, semi-taut and catenary mooring line. The first two are preferred in deep water because they have lighter weight, smaller foot-print and can better maintain the position of floating structure. However, it leads to large angle between the axial and horizontal direction. As a result, they demand anchor with higher holding capacity. To reduce the weight of a mooring line, the traditional steel cable has

---

This thesis follows the style of Ocean Engineering.

been partially replaced by synthetic ropes, such as, polyester ropes in deep water. As flexible as it is, the catenary mooring lines are incapable of resisting compression loading with their two ends connecting to seafloor, through an anchor, and floating structure, respectively. Thus, as a floating structure moves and rotates, the position of touch down point (TDP) of a mooring line varies and the mooring line profile changes. All these features, associated with the motion of a mooring system itself, lead to final mooring forces in a highly-nonlinear manner.

During the interaction between a mooring line and the seafloor, the friction imposed on the lying portion of a mooring line affects both the profile and the dynamic tension in the mooring line. Consequently, the contact friction arising from relative motion between a mooring line and seafloor, which has been neglected in most studies, contributes to the mooring force at the fairlead.

On the other hand, in the design of steel catenary risers (SCR), the contact interaction that has been mentioned above, along with embedment and trenching effect, is considered to be a critical issue. However, in this study, we focus on the bottom friction on the mooring line.

1.2 Review of previous work

Several models were used to simulate the interaction between seafloor and mooring line. There were both frequency-domain model (Triantafyllou et al., 1985) and time-domain model (Teng and Wang, 1995) by truncating the mooring line at TDP and attaching it to a linear spring and/or dash pot. However, these models become invalid when it comes to large dynamic motions about the static TDP. In developing a dynamic analysis method, Thomas (1993), used a lumped-mass method and considered the seafloor as a rigid bottom. Recently, the seafloor is commonly modeled as an elastic foundation, following Inoue and Surendran (1994) and Webster (1995).

However, only a few of the models accounted for in-plane friction between mooring line and seafloor. Thomas simulated the bottom friction in both tangential and normal directions with an empirical model, which considers bottom friction and allows the increase in friction due to embedment of a mooring line at seafloor. The results showed that, by including the bottom friction, no significant changes were observed from peak value, trough value and average of the tension at the fairlead. Liu and Bergdahl (1997) simulated bottom friction with an extended Coulomb model, in which the dynamic friction is ramped according to the velocity of the mooring line portion at the seafloor. Liu and Bergdahl also simulated the friction in frequency domain, in which a constant

friction is added to the governing equation and linearized when there is a nonzero velocity at the node contacting the seafloor. They finally came to the conclusion that bottom friction does increase the energy dissipation, which depends on the excitation amplitude at the fairlead.

In reality, when the portion of a mooring line moves at the seafloor, the bottom friction depends on several factors in addition to the vertical bottom support from the seabed. Different friction coefficients should be chosen according to the properties of the seafloor soil, such as sand, mud, clay, gravel, etc. Furthermore, Thomas considered the multipliers to give the effective contacting area in the normal and tangential directions, respectively, in computing the friction. The contacting area is related to the trenching development on the seabed as the mooring line slides from the left to the right repeatedly. Therefore, the material properties and the behavior of the seabed soil are required in order to simulate the bottom friction accurately. At this stage, these factors are not included in this study.

2. METHODS AND MODELS

2.1 Analytical solution for static problem

For benchmark checking, we derive an analytic solution for a mooring line whose fairlead is moving very slowly in the sway direction. Since it is moving very slowly, the hydrodynamic force applied on the mooring line and its own inertial force are neglected. The forces applied on the mooring line are the force at its fairlead, wetted weight (after subtract the buoyancy) and the bottom support and friction on the portion of the mooring line contacting the seabed soil. In essence, the analytic solution is for a mooring line with a static movement Y in the sway direction at its fairlead.

For simplicity, the following assumptions have been made in the derivation.

- The friction between the mooring line and the seafloor is in the tangent direction and small enough to be neglected in static analysis. In other words, only transverse friction is allowed.
- The mooring line is considered to be inextensible.
- The bottom friction is based on an original Coulomb model (see Figure 2), where μ is the bottom friction coefficient and N is the submerged weight of the mooring line per unite length.

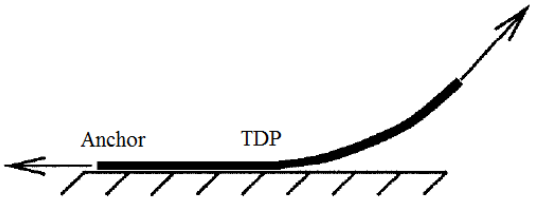

Figure 1 The mooring line with a portion lying on the seafloor, in side view.

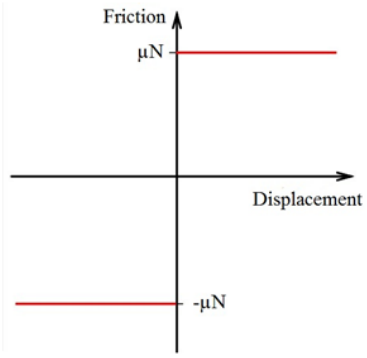

Figure 2 The original Coulomb model

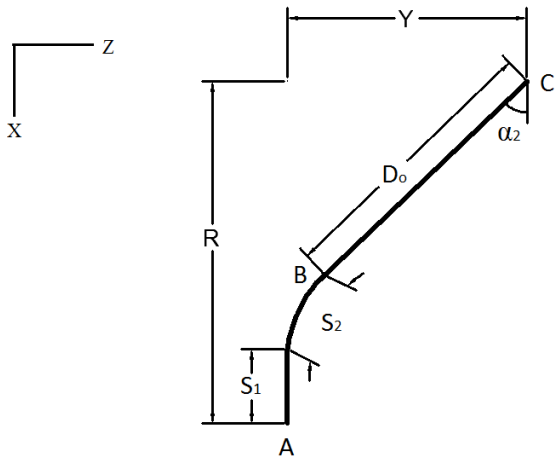

Figure 3 The top-view for profile of the mooring line for case 1.

Allowing for the bottom friction and the fairlead of a mooring line moving in its sway direction by distance Y, there are generally two cases of equilibrium. The top view of the two cases are shown in Figure 3and 5, respectively. For the first case shown in Figure 3, we have anchor point A, TDP at point B and fairlead at point C. The arc length of the mooring line is measured from point A. S_1 denotes the arc length of mooring line resting on the seabed. S_2 denotes the arc length of the mooring line with bottom friction imposed on it. R is equal to the horizontal excursion of the mooring line and D_0 is the horizontal distance between TDP and fairlead. Obviously, the part of mooring line S_2 is resting on the seafloor and imposed with bottom friction.

By taking an element of the length ds, which belongs to the segment S_2, the force equilibrium in transverse direction gives (see Figure 4):

$$2T \sin\frac{\Delta\alpha}{2} = F_{ft}\, ds \tag{1}$$

where T represents the tension and F_{ft} refers to the bottom friction. α denotes the tangential angle relative to the x axis.

Since $\Delta\alpha$ is very small, we have:

$$2T \sin\frac{\Delta\alpha}{2} \cong T\Delta\alpha \tag{2}$$

thus,

$$T \cdot \alpha = F_{ft} ds \tag{3}$$

let ds go to 0, we have

$$\frac{d\alpha}{ds} = \frac{F_{ft}}{T} \tag{4}$$

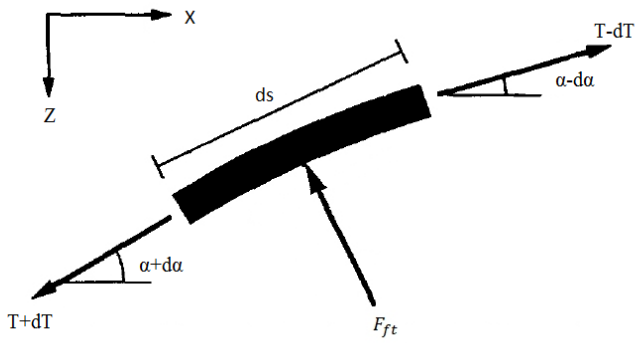

Figure 4 The force equilibrium of an element in transverse direction. The top-view of the element with surge direction X and sway direction Z with non-zero offset.

according to the third assumption, we have:

$$F_{ft} = \mu N \tag{5}$$

taking the tension T as a constant, as mentioned in the last assumption,

$$\alpha(s) = \frac{\mu N s}{T} - \frac{\mu N S_1}{T} \tag{6}$$

Considering geometry relations, in x direction and z direction respectively:

$$R = \int_{S_1}^{S_2+S_1} \cos\alpha \, ds + D_0 \cos\alpha_2 + S_1 \tag{7}$$

$$Y = \int_{S_1}^{S_2+S_1} \sin\alpha \, ds + D_0 \sin\alpha_2 \tag{8}$$

where,

$$\alpha(S_1) = 0 \tag{9}$$

$$\alpha_2 = \alpha(S_2 + S_1) = \frac{\mu N}{T} S_2 \tag{10}$$

we obtain:

$$R = \frac{T}{\mu N} \sin\alpha_2 + D_0 \cos\alpha_2 + S_1 \tag{11}$$

$$Y = \frac{T}{\mu N} (1 - \cos\alpha_2) + D_0 \sin\alpha_2 \tag{12}$$

Additionally, by adopting the classic catenary equations, which ignore the extension as the second assumption:

$$D_0 = \frac{T}{N} \sinh^{-1}\left[\frac{N(S_0 - S_2 - S_1)}{T}\right] \tag{13}$$

$$H = \frac{T}{N}\left[\cosh\frac{N D_0}{T} - 1\right] \tag{14}$$

where, T is horizontal component of the tension at fairlead (T is equal to the tension for the mooring line resting on the seafloor), H is the vertical distance from fairlead to TDP and S_0 is the total length of the mooring line. We can finally solve the system of five nonlinear equations (from equations (10) to (14)) for five unknowns T, S_1, S_2, α_2, D_0 and then obtain tensions and profile along the mooring line.

As illustrated in Figure 5, the second case generally follows the same scheme as the first case. The only difference is that the unknown S_1 is replaced by the unknown α_1, which is the angle at anchor point. Then, the equations from (10) to (14) become:

$$\alpha\left(S_2\right)=\frac{\mu N}{T}S_2+\alpha_1=\alpha_2 \tag{15}$$

$$R=\frac{T}{\mu N}\left(\sin\alpha_2-\sin\alpha_1\right)+D_0\cos\alpha_2 \tag{16}$$

$$Y=\frac{T}{\mu N}\left(\cos\alpha_1-\cos\alpha_2\right)+D_0\sin\alpha_2 \tag{17}$$

$$D_0=\frac{T}{N}\sinh^{-1}\left[\frac{N\left(S_0-S_2\right)}{T}\right] \tag{18}$$

$$H=\frac{T}{N}\left[\cosh\frac{N D_0}{T}-1\right] \tag{19}$$

Here, the equations are solved numerically with a program in Matlab version. The results will be discussed in section 4.1.

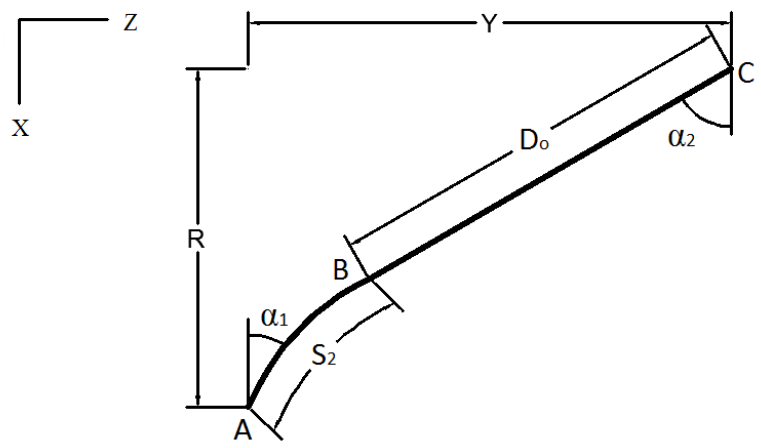

Figure 5 The top-view for profile of the mooring line with non-zero offset. The deflection angle at anchor point is non-zero.

2.2 Model description

In dry contacts, two effects are involved: the sticking effect and sliding effect. The former one happens when the friction is applied without any sliding at the interface of contact. In short, the sticking effect comes with the static friction. While the latter means the friction is caused by the actual sliding between two contacting bodies. In this study, the transverse friction was modeled based on the original Coulomb model in time domain (see Figure 2), which was widely used to model the sliding effect in a mechanical system, such as ball and bearing systems. The basic idea is to set a ramp displacement threshold. The bottom friction increases linearly to the displacement before the displacement exceeds the threshold and the maximum friction is reached.

2.2.1 Static model

In a static simulation, the Coulomb model is extended by introducing a ramp to the displacement. As the portion of a mooring line lying on the seabed moves away from its static position, the transverse friction imposed on the elements increases linearly to the displacement (in transverse) relative to their static position and current position. This friction will not be fully loaded until the displacement exceeds C_d, known as the ramp displacement threshold (see Figure 6). In order to get a stable simulation, we take C_d to be the nominal radius of the mooring line after trial and error.

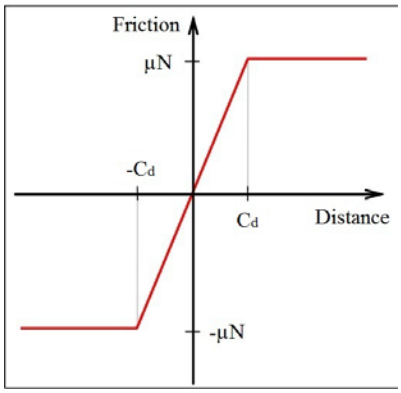

Figure 6 Coulomb model with a ramp to the displacement.

2.2.2 Dynamic model

In a dynamic analysis, the bottom friction is determined by the combination of models with ramps to displacement and velocity respectively. The value of the friction is determined by the following rules:

1. Nodes will be considered to be at rest if their current velocities are smaller than 1e-8 m/s, the meaningful velocity. Before this value, the velocities are considered to be numerical noises and the friction keeps the same magnitude as that in the previous time step. For example, if at the previous time step, the friction coefficient is zero, than the coefficient remains zero.
2. Once the velocities become greater than the meaningful velocity, the nodes start to move. When the velocities are between the meaningful velocity and C_v, the ramp velocity threshold, the friction increases linearly to the velocity (in transverse). Similarly, when the velocities are greater than C_v, the maximum friction is reached.
3. When the displacement is larger than 1e-4 m, another value of friction will be assessed based on the model plotted in Figure 6. The actually value of friction is determined by the larger one between those obtained based on models described in Figure 6 and Figure 7. Here the value of 1e-4 is also picked up for numerical stability.
4. Finally, the values of friction coefficient will be greater or at least equal to that of the last time step, unless a node begins to move towards the opposite direction.

The above model for determining the friction coefficient is able to include the sticking effect by maintaining the value of friction at least equivalent to that of the previous time step in situations where the static friction occurs. For example, from step 10 to step 20, if the node reverses at step 18, the nodes will probably stand still at the steps right before step 18 although the friction may be still pretty big. Furthermore, the reverse sliding behavior of the mooring line on the seafloor can be accounted properly by ramp function of the friction value according to both the velocity and the displacement instead of the displacement only. Apparently, the displacement directly relies on the length of time step, which varies when different lengths of time step or different excitations at the fairlead. This variability makes it difficult to choose the tolerance value for the ramp.

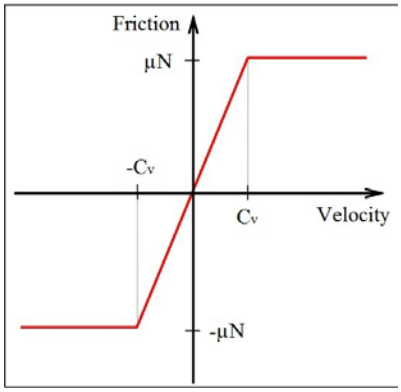

Figure 7 Coulomb model with a ramp to the velocity.

2.3 Numerical implementation

The methods most frequently employed for the dynamic simulations of the slender rod structure include the lumped parameter (mass) method (Leonard and Nath, 1981) and the FEM (Webster, 1975). The code CABLE3D, by Ma and Webster (1994), Chen et al. (2001), is developed based on the later scheme. While in this study, the mooring line analysis part of CABLE3D is translated from FORTRAN language into Matlab language with the same numerical scheme. The comparisons between the static and dynamic simulations obtained using these two versions show almost identical result. These comparisons are omitted for brevity.

2.3.1 Governing equation and tangential bottom friction

The CABLE3D employs the dynamic equations based on the conservation of linear momentum and moment of momentum. Two models for slender rod are featured here: the bar model and the beam model. The former considers the extension of an element but neglects the bending moment while the latter considers the bending moment but neglects the extension. Using a global-coordinate-based nonlinear FEM method, originally induced by Garrett (1982), the governing equations are then discretized with the Galerkin's scheme. Therefore, the partial differential equations become a set of

nonlinear ordinary differential equations. In static analysis, terms related to the time derivatives are equal to zero. The nonlinear equations then are solved using the Newton's method. While in dynamic simulation, an implicit scheme is used. That is, the Newmark-β time integration scheme (Newmark, 1959) is used to solve for the nodal displacement and tension increment of all the elements at each time step.

In the version of CABLE3D, given by Chen (2002), the bottom friction is considered only in axial direction as an external force, which is therefore treated as an extra term, q^{Frict} in the governing equation. The model for this friction is based on the ramp of velocity following Lindahl and Sjöberg (1983), which is essentially the same with the model plotted in Figure 7.

$$q^{Frict} = \begin{cases} C_f \mu NS \dfrac{\mathbf{r}'}{(1+\varepsilon)} & D - (\mathbf{r}\cdot\mathbf{e}_y - D_{btm}) > 0 \\ 0 & D - (\mathbf{r}\cdot\mathbf{e}_y - D_{btm}) \le 0 \end{cases} \tag{20}$$

$$C_f = \begin{cases} -1 & v_t > C_v \\ -\dfrac{v_t}{C_v} & |v_t| \le C_v \\ 1 & v_t < C_v \end{cases} \tag{21}$$

where v_t is the velocity of the node in axial direction, μ is the bottom friction coefficient and C_v is the ramp velocity threshold. $\mathbf{r}$ represents the position of the node and $\mathbf{r}'$ is the partial derivative relative to the arc length of the mooring line, which is hence the unit tangent vector. D_{btm} equals to the bottom depth, D is the

radius of the mooring line and N denotes the submerged weight per unit length. ε accounts for the axial strain of the mooring line.

2.3.2 Static problem

In our study, the existing CABLE3D is extended to consider the transverse bottom friction. In simulating the bottom friction in a static analysis, the implementation is shown below based on the model in Figure 6:

$$q^{Frict} = \begin{cases} C_f \mu N \dfrac{\mathbf{t}}{(1+\varepsilon)} & D - (\mathbf{r}\cdot\mathbf{e}_y - D_{btm}) > 0 \\ 0 & D - (\mathbf{r}\cdot\mathbf{e}_y - D_{btm}) \le 0 \end{cases} \tag{22}$$

$$C_f = \begin{cases} -1 & \mathbf{r}\cdot\mathbf{e}_z > C_d \\ -\dfrac{|\mathbf{r}\cdot\mathbf{e}_z|}{C_d} & |\mathbf{r}\cdot\mathbf{e}_z| < C_d \\ 1 & \mathbf{r}\cdot\mathbf{e}_z < -C_d \end{cases} \tag{23}$$

where C_d is the ramp displacement threshold and $\mathbf{t}$ is the unit normal vector. In this study, C_d equals to the nominal radius for numerical stability concern.

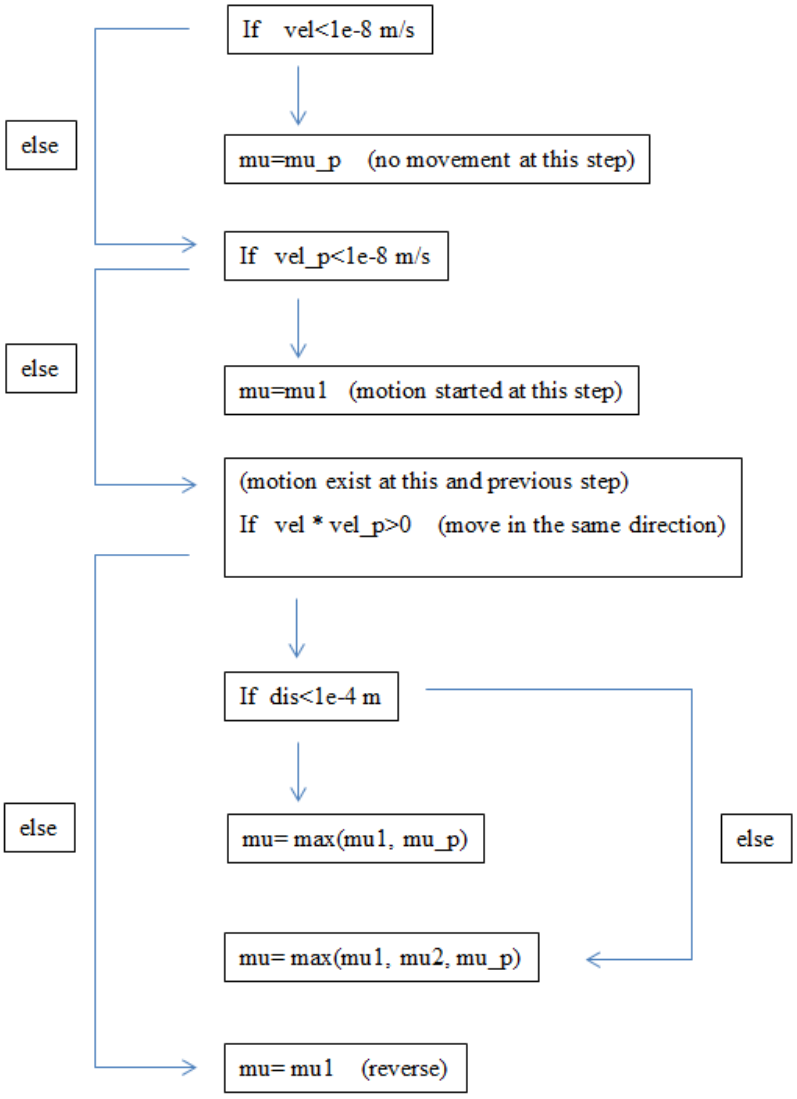

Figure 8 Flow chart for the simulation of bottom friction in dynamic analysis

2.3.3 Dynamic problem

The basic principles for determining the transverse bottom friction were stated in section 2.2.2. The implement of the two models in our code is depicted in the following flow chart (Figure 8).

In the flow chart above, “vel” and “vel_p” denote the velocity for the current and previous time step, respectively. “mu” and “mu_p” represent the bottom friction coefficient in the current and previous time step. “dis” refers to the displacement relative to the static position. The static position refers to either the initial position of the node or the position in the first time step after the transverse moving direction of node reverses. For example, the velocity in time step 10 and time step 11 have opposite directions, which means the direction of a node reverses. Then the position in time step 11 becomes the static position until the next static position arises. “mu1” is the friction coefficient obtained based on the model described in Figure 7 and “mu2” is the friction coefficient based on the model showed in Figure 6. The value of 1e-8 m/s is the meaningful velocity, smaller than which the velocities are considered to be numerical noise.

2.4 Description of Orcaflex

An element along a mooring line is modeled by a lumped mass method in Orcaflex. The mass of the mooring line is concentrated on a series of nodes and the parts between the nodes are considered to be massless springs. As a result, those springs make up the whole mooring line with its mass only distributed at the nodes.

In a static analysis, the equilibrium configuration is determined by an iterative method. The effects of bending and torsional stiffness of the line are set to be zero. In a dynamic analysis, the equations of motion are obtained and solved with the Generalized-α integration scheme (Chung, 1993). This scheme follows that, after solving for the acceleration vectors of each node, new velocities and positions will be updated at the end of the time step.

The bottom friction effect is also modeled with a Coulomb friction model similar to that depicted in Figure 6. A ramp is applied in the model to avoid the jumps resulting from the change of bottom friction. This linear ramp is a function of the displacement relative to the target position, which is defined and updated at the end of each time step. When the displacement is greater than the ramp displacement threshold C_d, the maximum friction coefficient is reached.

3. CASES FOR COMPARISON

Table 1
Physical properties and site information for Cases 1 and 2.

Cases	Case 1	Case 2
Length of mooring line	711.3 m	902.2 m
Elastic stiffness (EA)	1.69e9 N	3.84e8 N
Line weight in air	3.587e3 N/m	7.623e2 N/m
Line weight in water	3.202e3 N/m	6.981e2 N/m
Nominal mooring line diameter	0.14 m	0.09 m
Horizontal excursion	683.26 m	848.67 m
Vertical distance from fairlead to seafloor	82.5 m	250 m
Water depth	95 m	320 m

In the numerical simulation, three typical cases will be studied to verify the application of the friction model used in CABLE3D. The first one represents a shallow water case with a water depth of 95 m and more than 500m of the mooring line is lying on the seafloor. In the second case, a mooring line is deployed in water with an intermediate depth of 320m. More than 100 m of the mooring line contacts with the seafloor. The first two mooring lines are catenary mooring line of uniform material, while the last case is a semi-taut mooring line. It is installed with a water depth of 1100

m and composed of steel chain, wire and steel chain. About 270 m of the mooring line is lying on the seafloor.

Table 2 Physical properties and site information for Case 3.

Line segment	Top chain	Wire	Ground chain
Length of mooring line	76.2 m	1828.8 m	762 m
Elastic stiffness	9.759e8 N	1.212e9 N	9.759e8 N
Line weight in air	2.673e3 N/m	7.198e2 N/m	2.673e3 N/m
Line weight in water	2.326e3 N/m	5.703e2 N/m	2.326e3 N/m
Nominal mooring line diameter	0.1524 m	0.1905 m	0.1524m
Pretension	3.72e6 N		
Vertical distance from fairlead to seafloor		1100 m	
Water depth	1000 m		

The first case and second case were originally presented by Brown et al. (1997) and Jonkman (2009) respectively. The deep water case came from a 12-leg catenary mooring system with drag embedment anchors for a Gulf-of Mexico production semisubmersible platform (Wu, 1999). Detailed information of the mooring line in each case is summarized in Table 1 and Table 2.

In the demonstration of the static simulation in CABLE3D, the intermediate water case (Case 2) will be utilized, after which, dynamic simulations will be conducted for all

three cases using CABLE3D and Orcaflex respectively. For the comparison of the effect of the bottom friction, attention is paid to the tension at fairlead, its component in sway direction and the motion of sliding nodes right after the TDP, which is the first node after the TDP. The TDP may move along the mooring line following the motion at the fairlead, while the node we choose always contacts the seafloor. Besides, three different excitations at the fairlead are considered in the dynamic analysis, which are described below:

Excitation 1: a harmonic excitation with a period of 5s and amplitude of 1m in sway direction.

Excitation 2: a harmonic excitation with a period of 15s and amplitude of 3m in sway direction.

Excitation 3: a superposition of excitation 1 and excitation 2 in sway direction.

In Cases 1 and 2, when the bottom friction effect is not considered, the pretensions given by CABLE3D and Orcaflex are slightly different. Bearing this in mind, the results from CABLE3D and Orcaflex are not plotted together. Additionally, a ramp function is inserted to each of the simulation for the first 30 seconds. But the result of the ramp stage is neglected in section 4.2.

4. RESULTS AND COMPARISONS

4.1 Static results comparison

First of all, we verify the validity of the methods and models with the comparison of the results from CABLE3D, Orcaflex and the analytical solution. As mentioned above, the intermediate water depth case is used as the example case here. The axial stiffness of this mooring line is increased up to a very large value. Particularly, the axial stiffness is set to be 3.84e14 N in CABLE3D. In Orcaflex, the simulation cannot converge if the axial stiffness is too big. Therefore, the axial stiffness value is 3.84e11 N. However, these stiffness values are big enough such that the mooring lines could be considered to be inextensible and thus the numerical solution could be compared with the analytical solution.

Figures 9 and 10 illustrate the total tension and its component in sway direction at fairlead, with bottom friction excluded. Obviously, both the total tensions and tensions in sway direction at fairlead from these 3 methods are quite close and in good agreement. The error, as shown in Figure 9, between the results from CABLE3D and the analytical solution is less than 1‰.

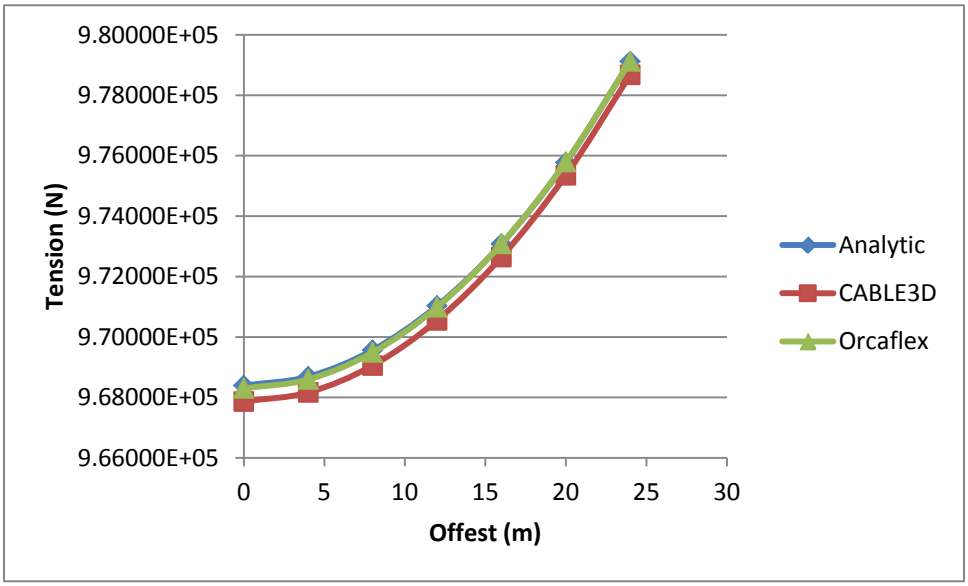

Figure 9 Total tension at fairlead. Bottom friction is not considered.

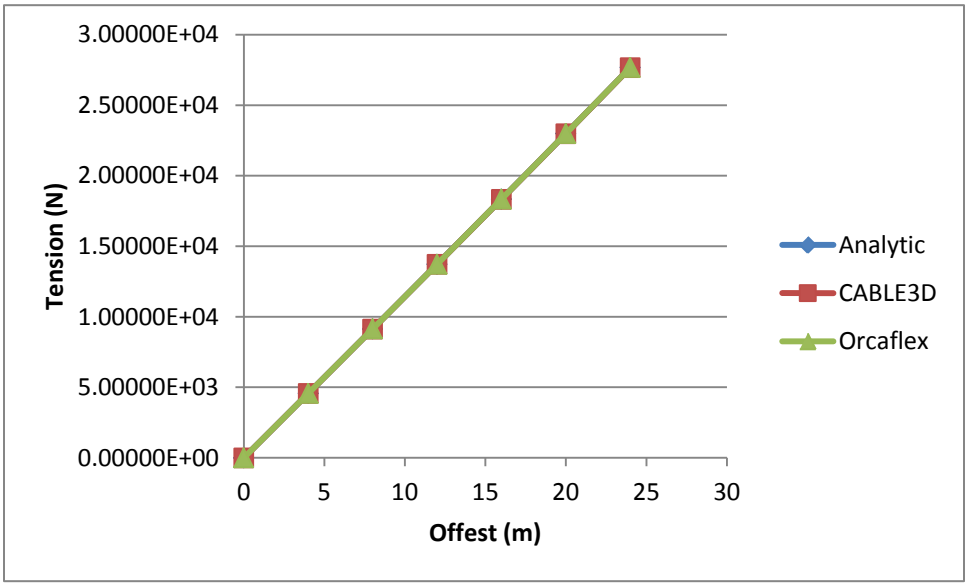

Figure 10 Tension in sway direction at fairlead. Bottom friction is not considered.

By including the bottom friction, as we can see from Figures 11 and 12 both of the total tension at the fairlead and its component in the sway direction increased a little bit. In Figure 11, the tension given by CABLE3D is about 1‰ smaller than that from the analytical solution. However, the tension in sway direction from the analytical solution is larger than those from numerical methods. As shown in Figure 12, the error between the results from CABLE3D or Orcaflex and the analytical solution can be as big as 17% when the offset is 24 m. This could be due to the ramp exists in the models of numerical schemes, which essentially reduces the friction effect for the purpose of the convergence in numerical simulations. However, the results from CABLE3D and Orcaflex are almost identical. Thus, we may come to the conclusion that the static part of CABLE3D is capable of simulating the bottom friction effect properly.

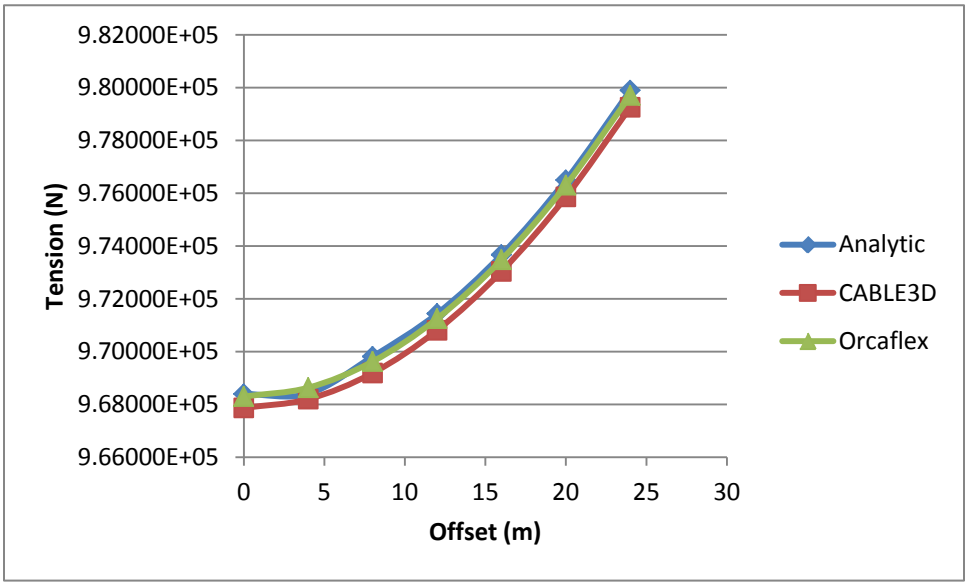

Figure 11 Total tension at fairlead. Bottom friction is considered.

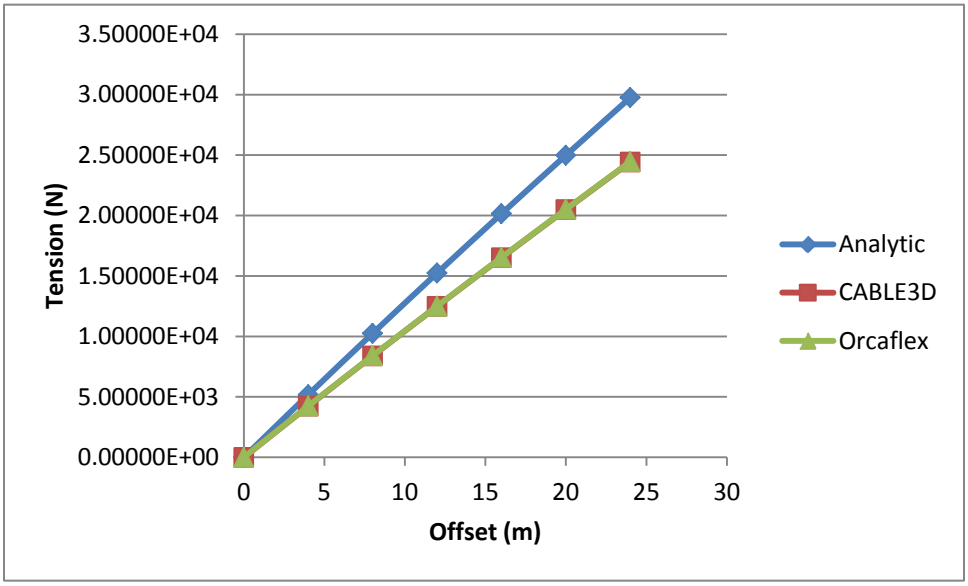

Figure 12 Tension in sway direction at fairlead. Bottom friction is considered.

As the verification of the dynamic part, a uniform excitation in sway direction at fairlead, with the velocity of 0.033 m/s, is imposed. The dynamic force of the mooring line is neglected because of the slow motion, making the results comparable with the analytical solution of static status.

With bottom friction effect excluded, it can be seen, from Figures 13 and 14, that the results of the total tension at fairlead are quite close, even though CABLE3D gives about 1‰ lower values. The tension components from two dynamic simulations and the analytical solution are almost the same. Also, Figures 15 and 16 show relation and trend of the curves similar to those in Figures 11 and 12. The only difference is that CABLE3D offers smaller tension component in sway direction compared with Orcaflex. As shown in Figure 16, the error between the results from CABLE3D and Orcaflex is less than 4%, which is acceptable.

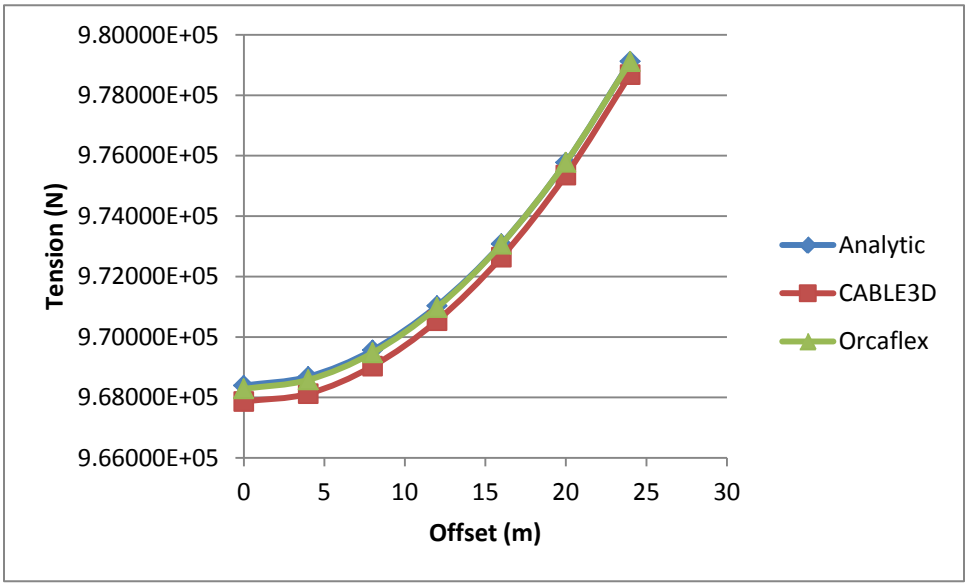

Figure 13 Total tension at fairlead. Bottom friction is not considered.

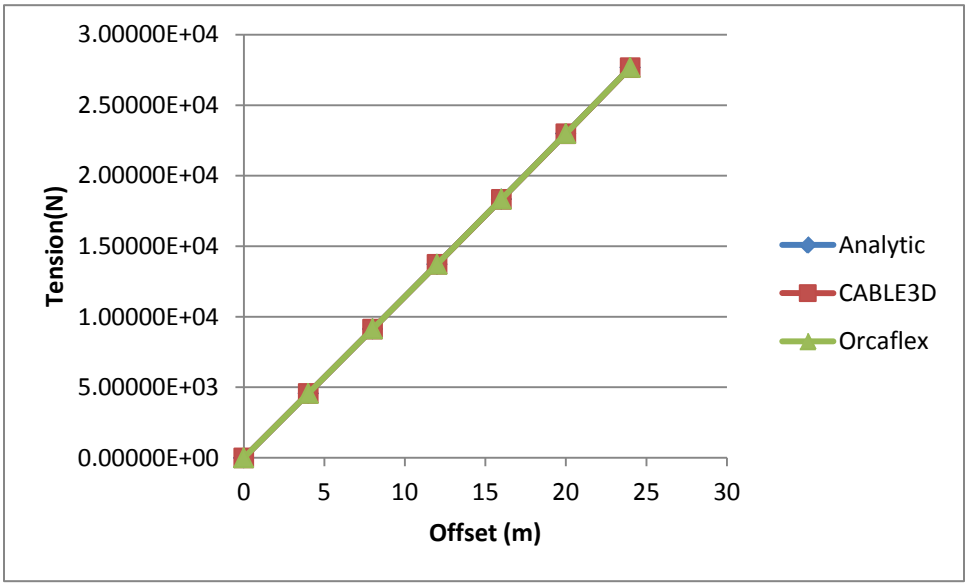

Figure 14 Tension in sway direction at fairlead. Bottom friction is not considered.

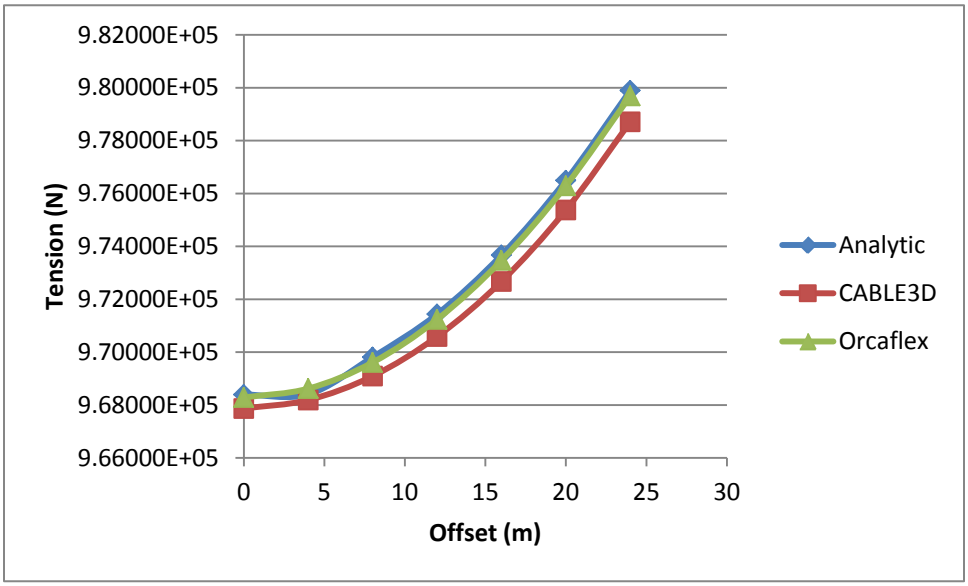

Figure 15 Total tension at fairlead. Bottom friction considered.

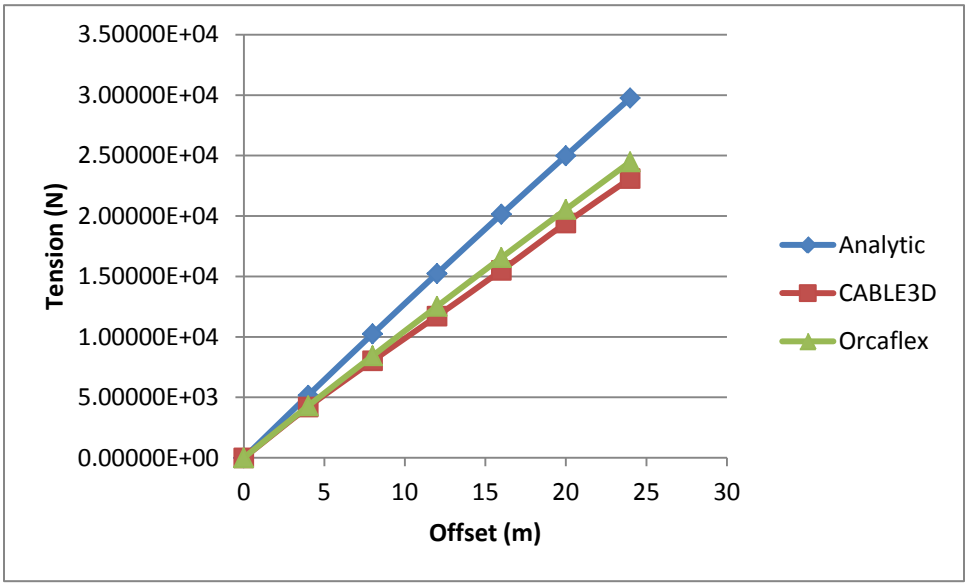

Figure 16 Tension in sway direction at fairlead. Bottom friction considered.

4.2 Dynamic results comparison

4.2.1 A mooring line in intermediate depth water

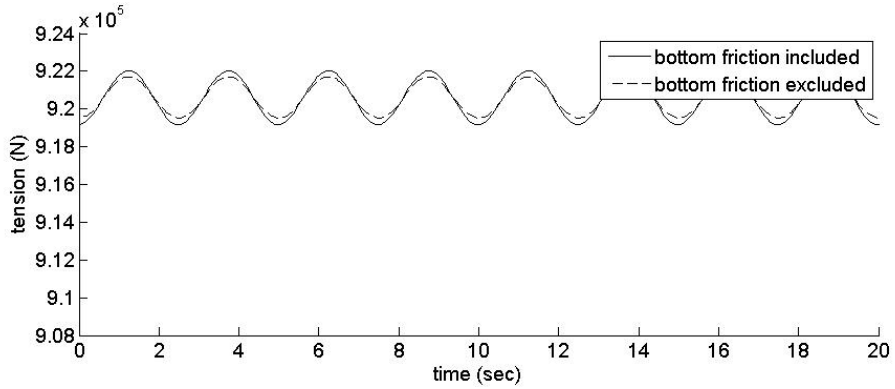

Figure 17 Total tension at fairlead under the excitation1. Result from CABLE3D for case 2.

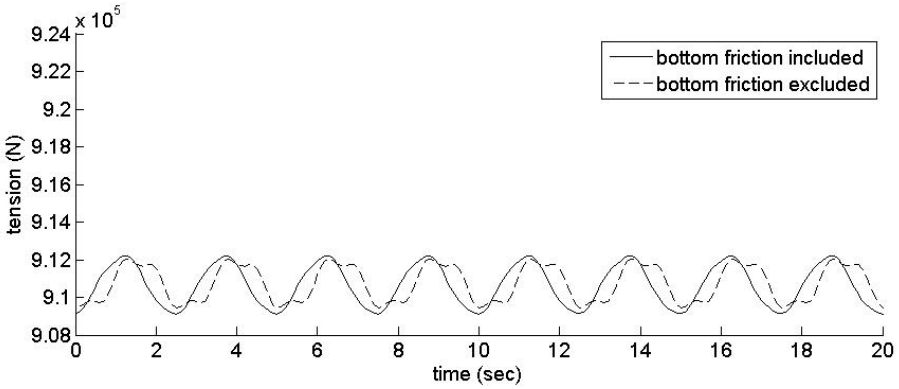

Figure 18 Total tension at fairlead under the excitation1. Result from Orcaflex for case 2.

Figures 17 and 18 show the effect of bottom friction on the tension at fairlead. Particularly, results from CABLE3D illustrate that the bottom friction leads peak values to be 0.35‰ higher and trough values to be 0.4‰ lower. While the Orcaflex predicts the peak and trough values 0.18‰ and 0.36‰ higher and lower respectively when taking the bottom friction in to account. Physically, however, the high-frequency energy from the result of Orcaflex is probably spurious, which does not appear when bottom friction is considered. Also, CABLE3D does not give the high-frequency response at all.

The fairlead tension component in sway direction, as shown in Figures 19 and 20, are almost the same no matter whether the bottom friction effect is considered or not. This is because that when the fairlead moves in sway direction, the angle between its axial axis and sway direction changes very little.

Compared the results in Figure 21 with Figure 22, the motions of the first nodes after TDP are almost the same when the bottom friction in not considered. Nevertheless, CABLE3D gives motion of a smaller amplitude when the bottom friction is considered, indicating that the nodes sliding on the seafloor are better constrained by bottom friction, while the maximum friction in their simulations are the same. Furthermore, the extra roughness shown in Figure 22 indicates that CABLE3D simulates the process more smoothly.

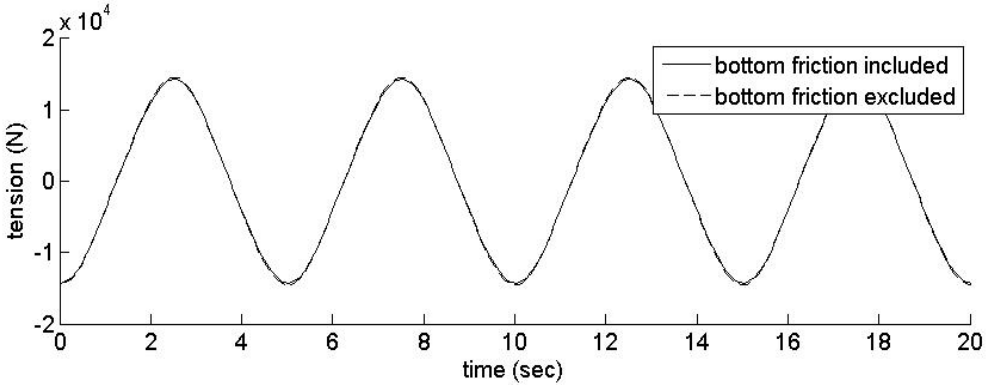

Figure 19 Tension in sway direction at fairlead under the excitation1. Result from CABLE3D for case 2.

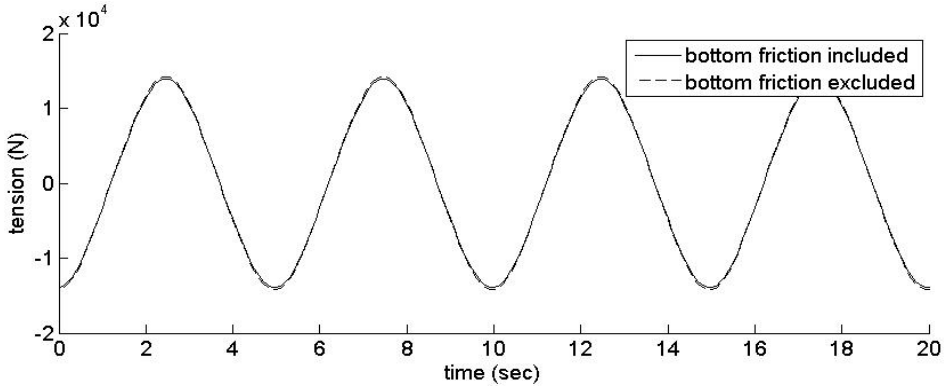

Figure 20 Tension in sway direction at fairlead under the excitation1. Result from Orcaflex for case 2.

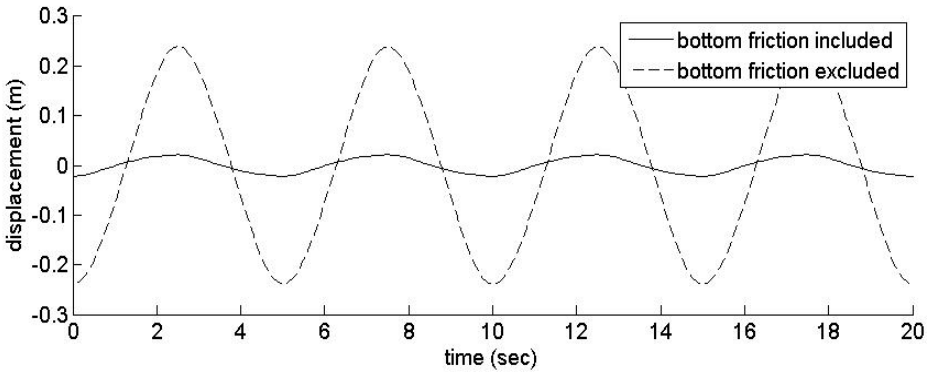

Figure 21 Displacement of the first node after TDP in sway direction under the excitation1. Result from CABLE3D for case 2.

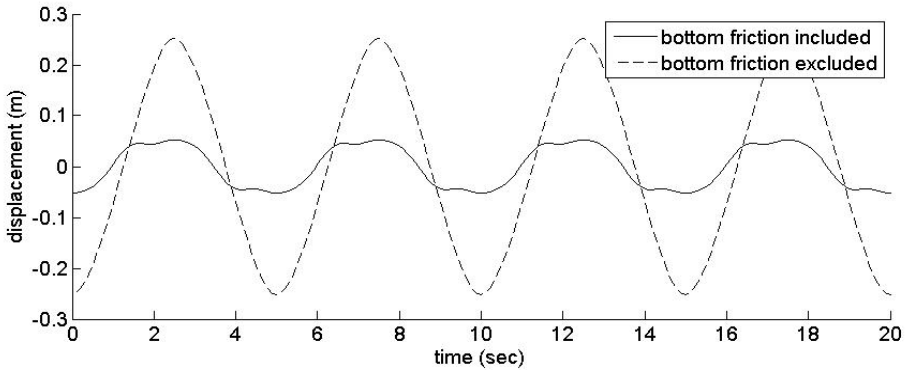

Figure 22 Displacement of the first node after TDP in sway direction under the excitation1. Result from Orcaflex for case 2.

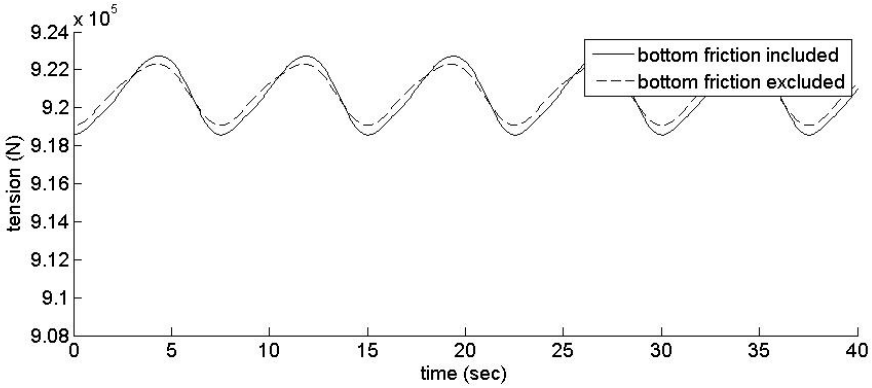

Figure 23 Total tension at fairlead under the excitation2. Result from CABLE3D for case 2.

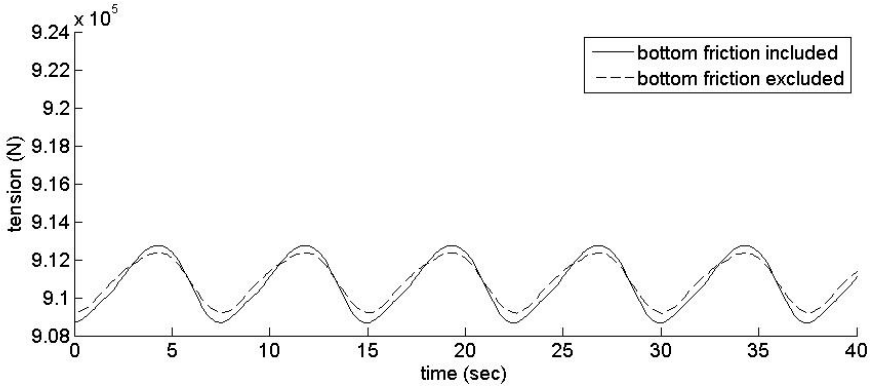

Figure 24 Total tension at fairlead under the excitation2. Result from Orcaflex for case 2.

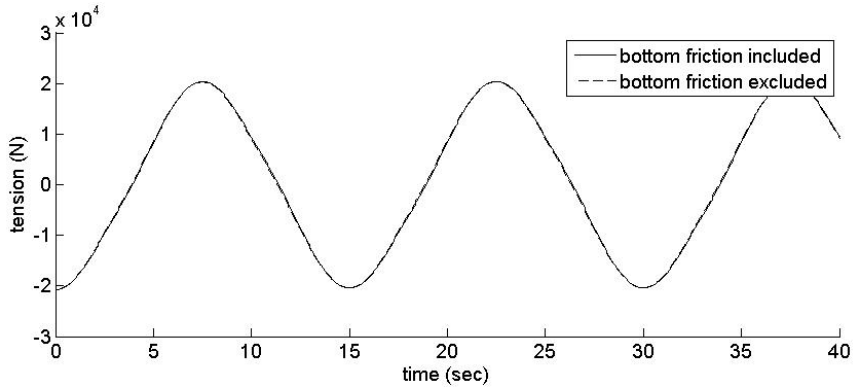

Figure 25 Tension in sway direction at fairlead under the excitation2. Result from CABLE3D for case 2.

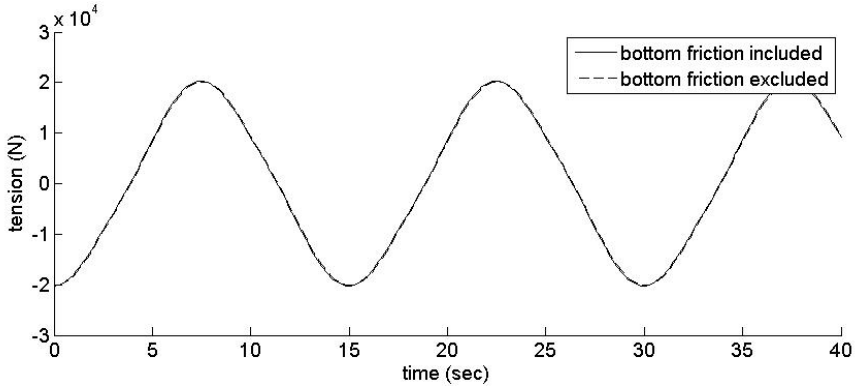

Figure 26 Tension in sway direction at fairlead under the excitation2. Result from Orcaflex for case 2.

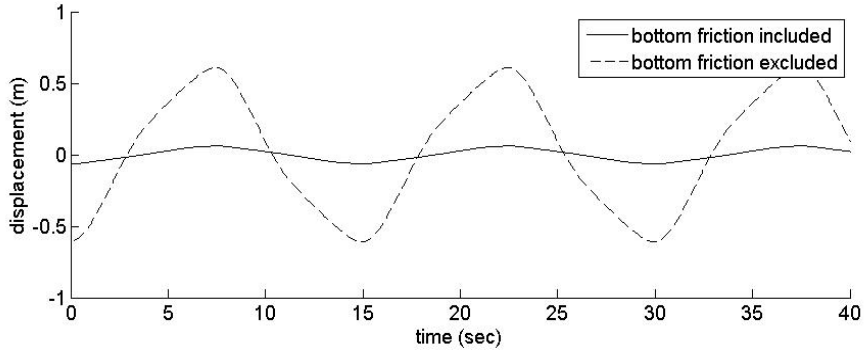

Figure 27 Displacement of the first node after TDP in sway direction under the excitation2. Result from CABLE3D for case 2.

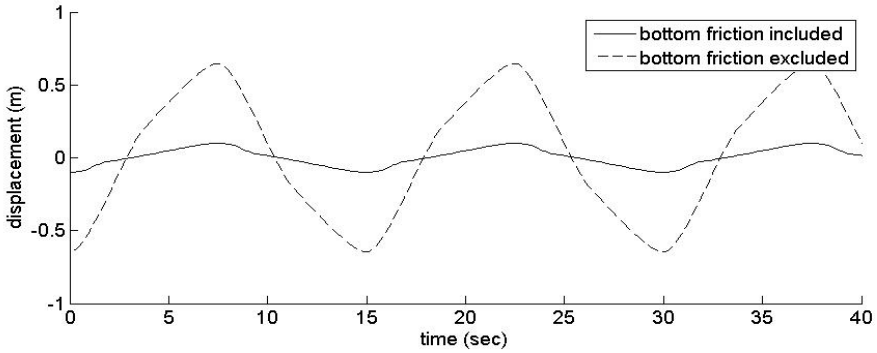

Figure 28 Displacement of the first node after TDP in sway direction under the excitation2. Result from Orcaflex for case 2.

Figures 23 and 24 show that under the excitation 2 at the fairlead in case 2, the bottom friction results in about 5‰ higher peaks and 4.5‰ lower troughs of the tensions at the fairlead. The corresponding components in the sway direction are almost identical, as illustrated in Figures 25 and 26, regardless that the bottom friction is ignored or considered. The node right after the TDP moves almost the same way by comparing the results from CABLE3D and Orcaflex except that CABLE3D gives a smooth curve after taking the friction effect into account, as shown in Figures 27 and 28.

With the excitation 3 imposed at fairlead, the results from CABLE3D and Orcaflex are in excellent agreement, as shown in the Figures from 29 to 34. The bottom friction did not produce significant differences about the tensions at the fairlead. We observe great roughness regarding the motion of the sliding node given by Orcaflex, which probably arise from its bottom friction model.

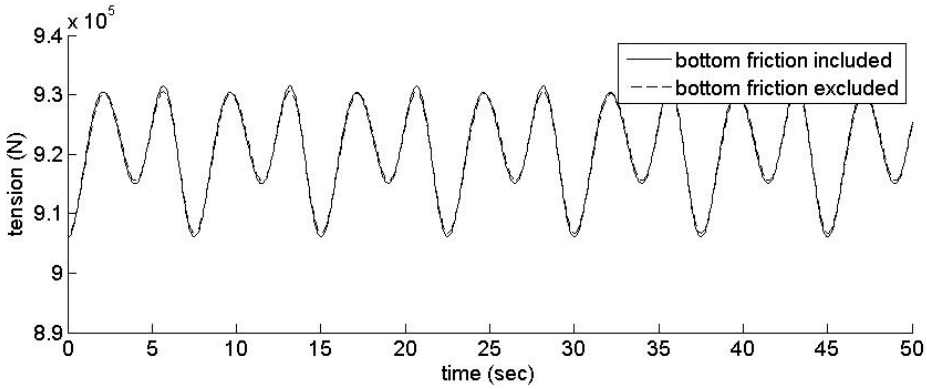

Figure 29 Total tension at fairlead under the excitation3. Result from CABLE3D for case 2.

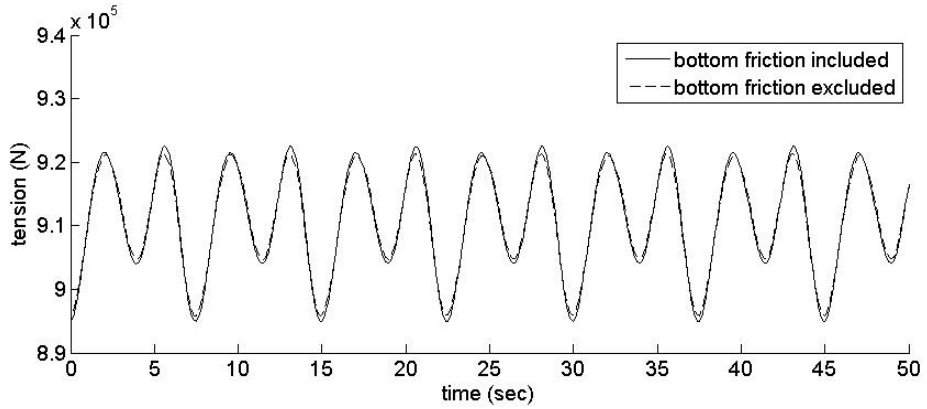

Figure 30 Total tension at fairlead under the excitation3. Result from Orcaflex for case 2.

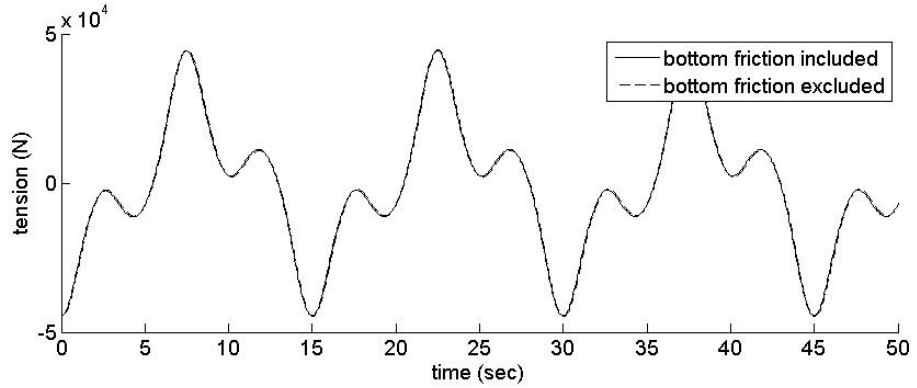

Figure 31 Tension in sway direction at fairlead under the excitation3. Result from CABLE3D for case 2.

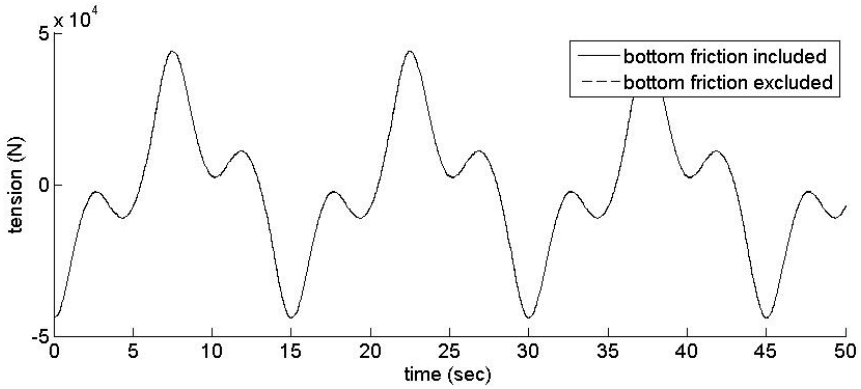

Figure 32 Tension in sway direction at fairlead under the excitation3. Result from Orcaflex for case 2.

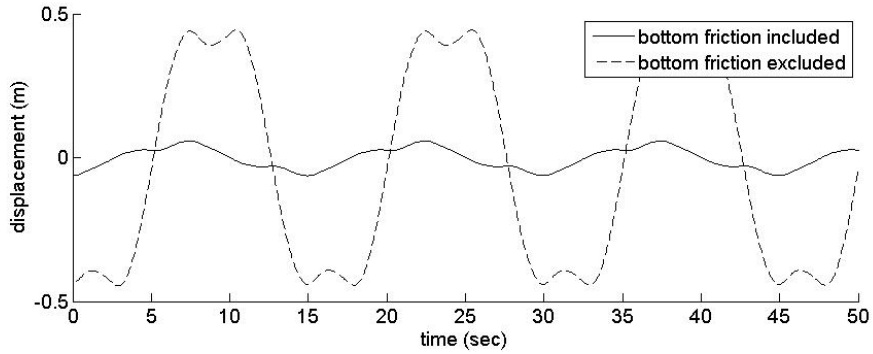

Figure 33 Displacement of the first node after TDP in sway direction under the excitation3. Result from CABLE3D for case 2.

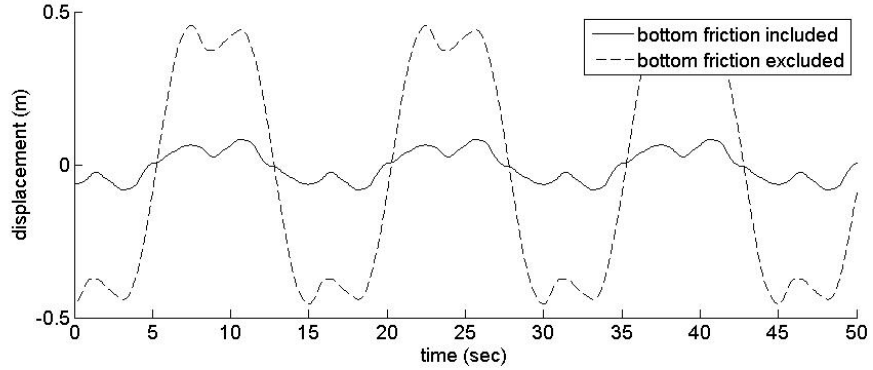

Figure 34 Displacement of the first node after TDP in sway direction under the excitation3. Result from Orcaflex for case 2.

4.2.2 A mooring line in shallow depth water

As shown in Figures 35 and 36, the bottom friction effect given by CABLE3D leads to 0.5% higher peaks and 0.6% deeper troughs of the total tension. More importantly, the dynamic force increased about 100% percent after considering the bottom friction, according to the result from CABEL3D. It is also obvious that the bottom friction leads the maximum value of the tension in sway direction to be about 11% higher, based on the observations of Figures 37 and 38. Regarding the sliding motion of the nodes at the seafloor, from Figures 39 and 40, CABLE3D gives motion of smaller amplitude and much flatter peaks and troughs. This behavior represents the sticking effect of the dry contact with static friction loaded on the mooring line, which is likely to happen when the node is about to move in the direction opposite to previous time steps.

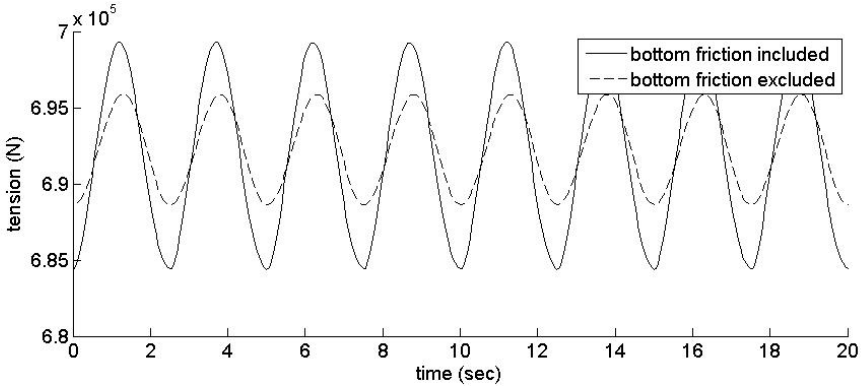

Figure 35 Total tension at fairlead under the excitation1. Result from CABLE3D for case 1.

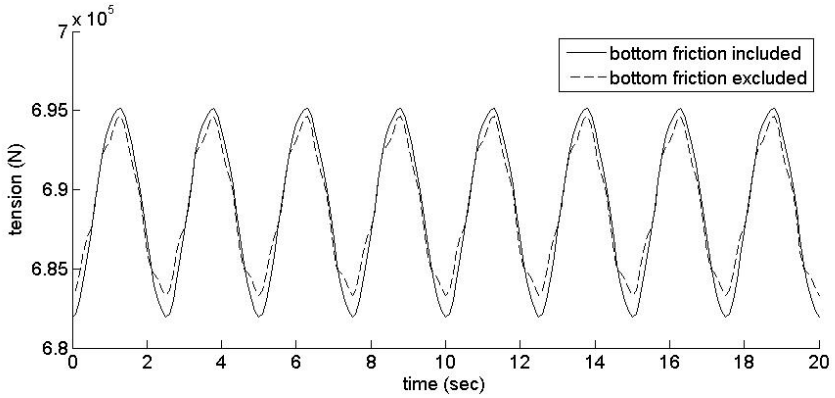

Figure 36 Total tension at fairlead under the excitation1. Result from Orcaflex for case 1.

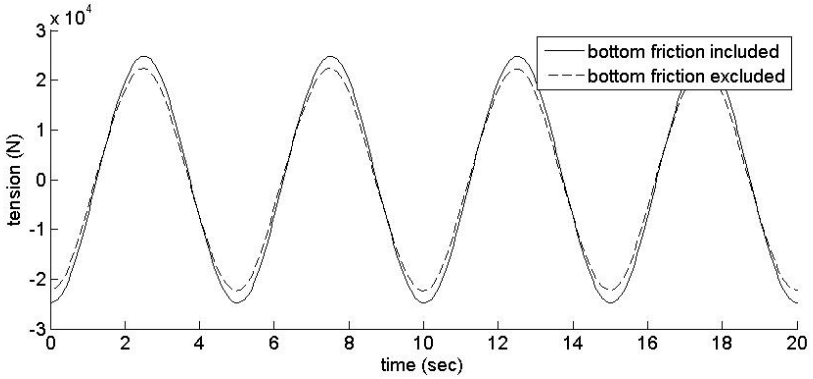

Figure 37 Tension in sway direction at fairlead under the excitation1. Result from CABLE3D for case 1.

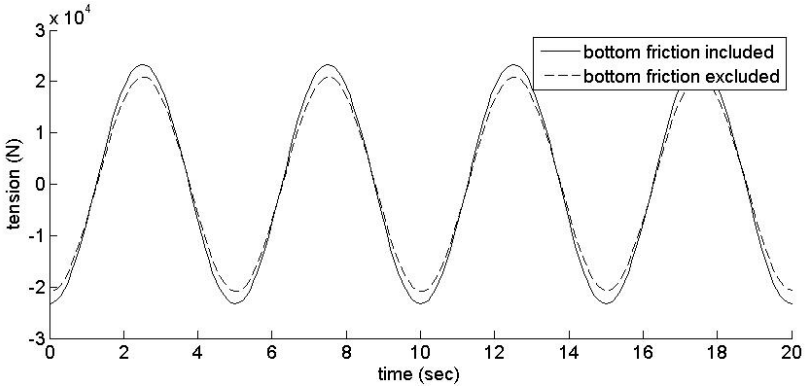

Figure 38 Tension in sway direction at fairlead under the excitation1. Result from Orcaflex for case 1.

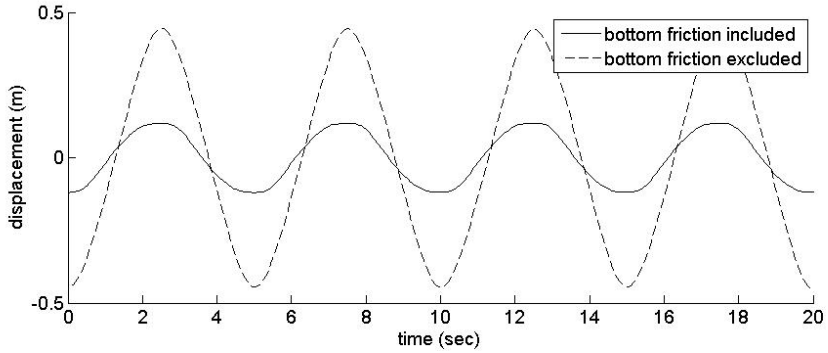

Figure 39 Displacement of the first node after TDP in sway direction under the excitation1. Result from CABLE3D for case 1.

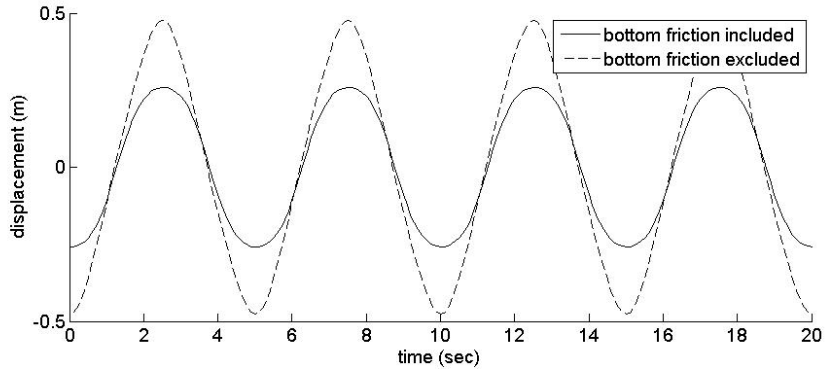

Figure 40 Displacement of the first node after TDP in sway direction under the excitation1. Result from Orcaflex for case 1.

With the excitation 2 at the fairlead, it is interesting to find that the tension becomes lower after taking the bottom friction into account, as in Figures 41 and 42. It might be because the motion of the mooring line sliding on the seafloor is in different phases with the motion of the fairlead. As a result, the bottom friction might be applied with the same direction as the force component at fairlead, cancelling out part of the force, and thus lead to a lower total force at fairlead. Besides, there exists clear high-frequency energy no matter whether the bottom friction is considered or not. Furthermore, Orcaflex predicts the motion of larger energy at high-frequency range. This high-frequency response may be due to different phases for the motion of different mooring line nodes, compared to the excitation at fairlead.

When it comes to the tension in sway direction and the sliding motion of the node, as illustrated in Figures from 43 to 46, we find the relation and trend of the curves are the same with those of the intermediate water case and other excitations. That is, the tensions in sway direction are quite close and the motion of the sliding nodes given by CABLE3D is a bit smaller when considering the bottom friction.

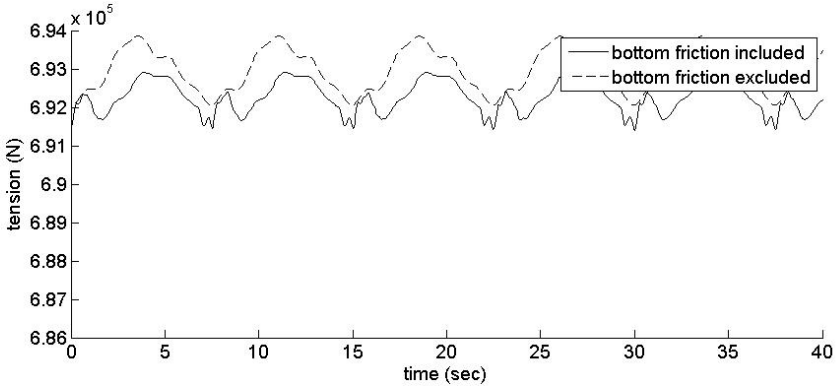

Figure 41 Total tension at fairlead under the excitation2. Result from CABLE3D for case 1.

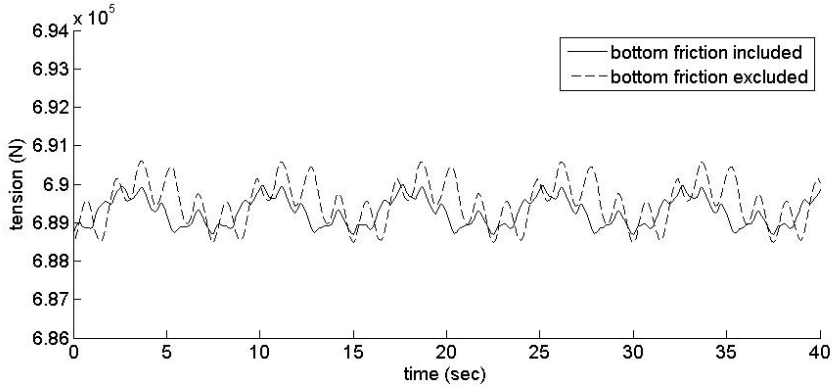

Figure 42 Total tension at fairlead under the excitation2. Result from Orcaflex for case 1.

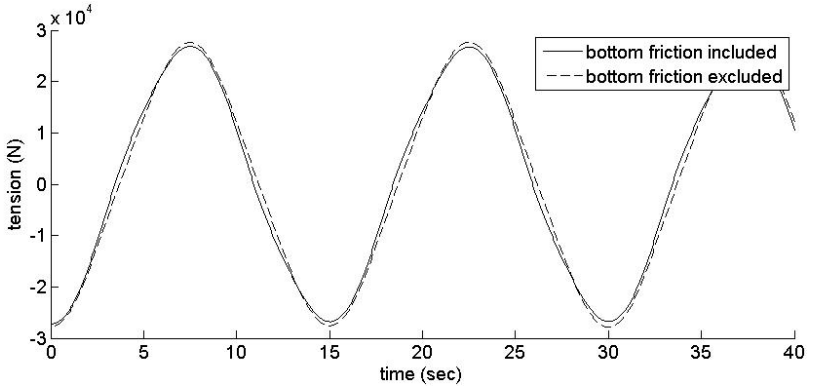

Figure 43 Tension in sway direction at fairlead under the excitation2. Result from CABLE3D for case 1.

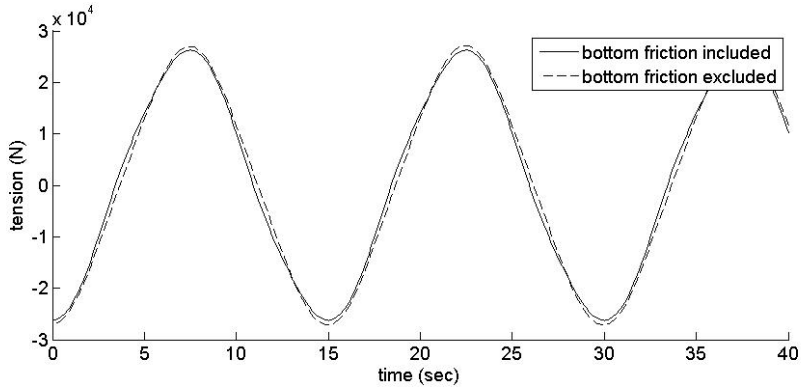

Figure 44 Tension in sway direction at fairlead under the excitation2. Result from Orcaflex for case 1.

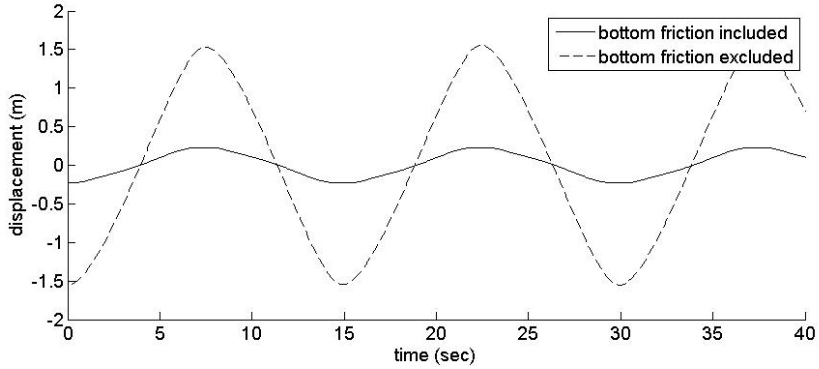

Figure 45 Displacement of the first node after TDP in sway direction under the excitation2. Result from CABLE3D for case 1.

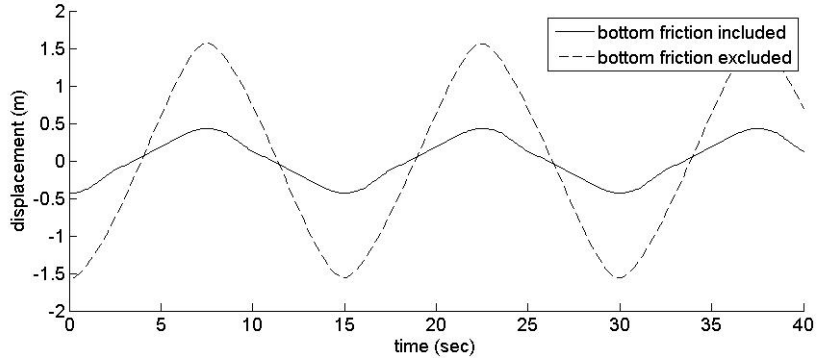

Figure 46 Displacement of the first node after TDP in sway direction under the excitation2. Result from Orcaflex for case 1.

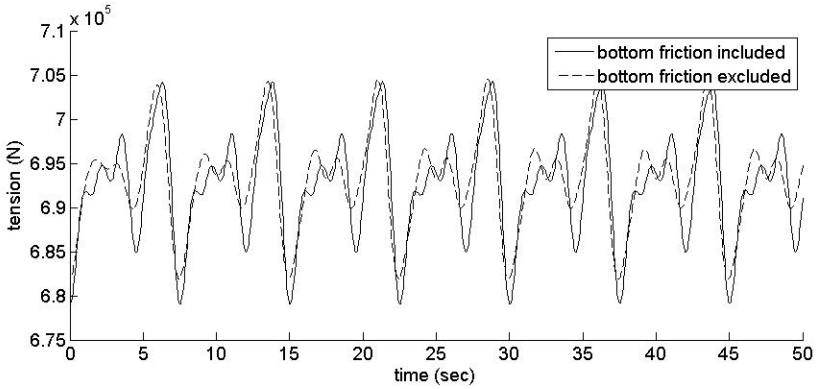

Figure 47 Total tension at fairlead under the excitation3. Result from CABLE3D for case 1.

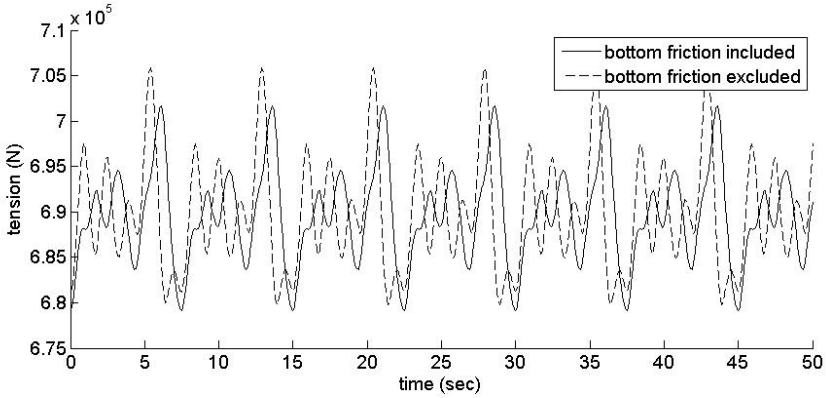

Figure 48 Total tension at fairlead under the excitation3. Result from Orcaflex for case 1.

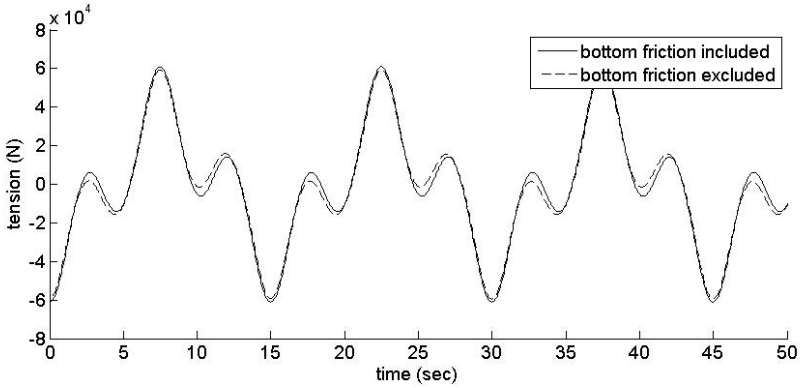

Figure 49 Tension in sway direction at fairlead under the excitation3. Result from CABLE3D for case 1.

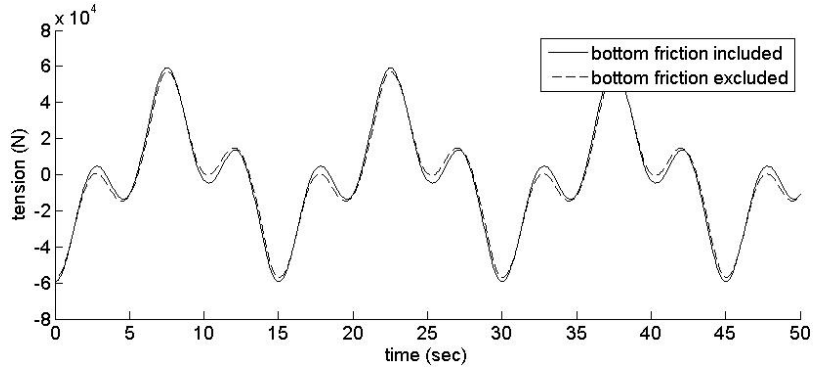

Figure 50 Tension in sway direction at fairlead under the excitation3. Result from Orcaflex for case 1.

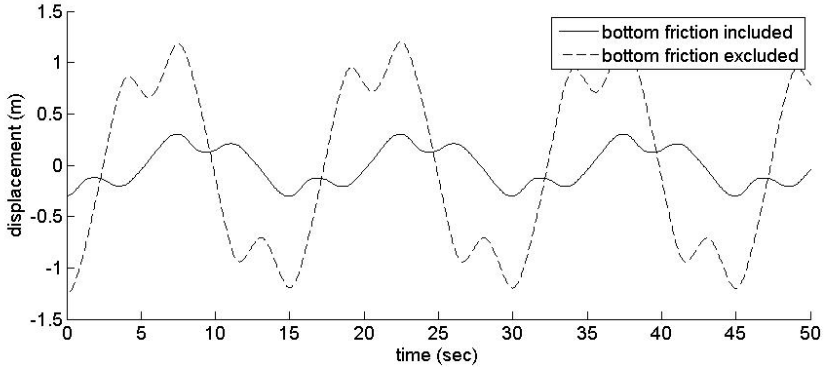

Figure 51 Displacement of the first node after TDP in sway direction under the excitation3. Result from CABLE3D for case 1.

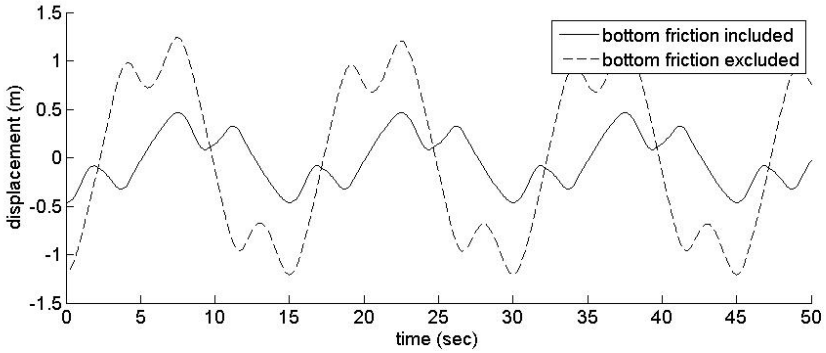

Figure 52 Displacement of the first node after TDP in sway direction under the excitation3. Result from Orcaflex for case 1.

With the superposition of the excitation 1 and excitation 2, as shown in Figures 47 and 48, Orcaflex gives a tension at fairlead with larger energy at the high-frequency range, compared to CABLE3D, although they share the same trend. The two figures also illustrate that CABLE3D offers a 0.4% lower minimum values and Orcaflex offers 0.8% higher maximum values for the tension at fairlead. From Figures 49 and 50, the difference of tension components in sway direction is also neglectable between with and without the consideration of bottom friction. Additionally, CABLE3D still gives the mooring line sliding motion with smaller amplitude, when considering the bottom friction, based on the observation of curves shown in Figures 51 and 52.

4.2.3 A mooring line in deep depth water

With the friction effect considered, the maximum of the total tension at fairlead slightly exceeds its peak value of that without the consideration of the bottom friction, predicted by CABLE3D as shown in Figure 53. While Orcaflex gives higher peak values and lower trough values of the tension when considering the friction effect, as illustrated in Figure 54. The high-frequency tension given by Orcaflex might be physically invalid because the excitation is only a harmonic motion.

The tension components in sway direction are in good agreement with those without the consideration of the bottom friction as shown in Figures 55 and 56. However, as the Figures 57 and 58 illustrated, Orcaflex gives larger peaks of motion for the sliding node. Similar to the previous results, the corresponding sliding motion including the friction has a great roughness, compared to the result from CABLE3D. The difference between the motion amplitudes is probably because of the huge water depth, along which the excitation energy dissipates. Also, the roughness is due to the model Orcaflex uses for modeling the friction. Particularly, in Orcaflex, the displacement used in the friction model is relative to the target position that may change discontinuously. As a result, jumps in the change of the displacement and the corresponding friction arise in the simulation.

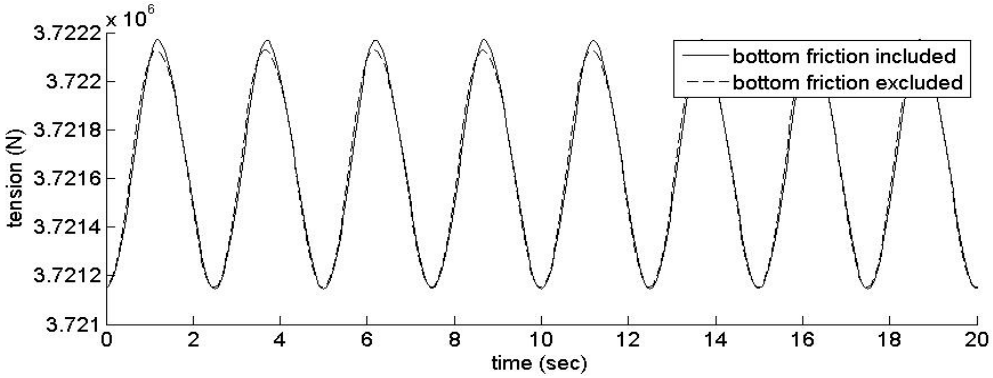

Figure 53 Total tension at fairlead under the excitation1. Result from CABLE3D for case 3.

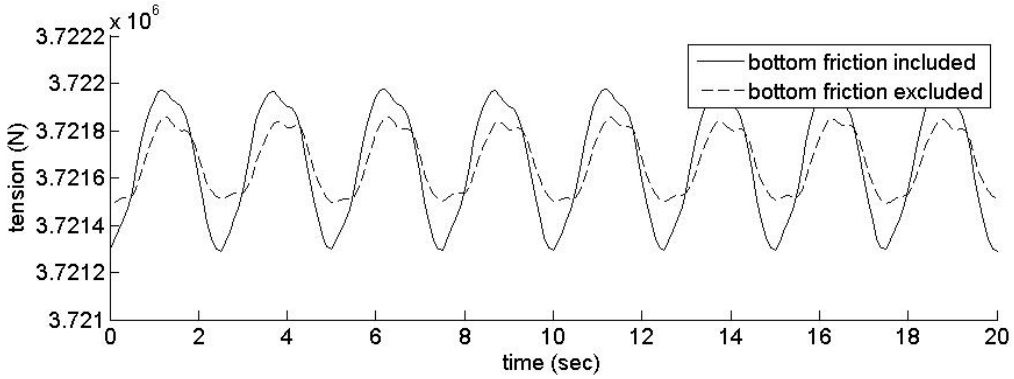

Figure 54 Total tension at fairlead under the excitation1. Result from Orcaflex for case 3.

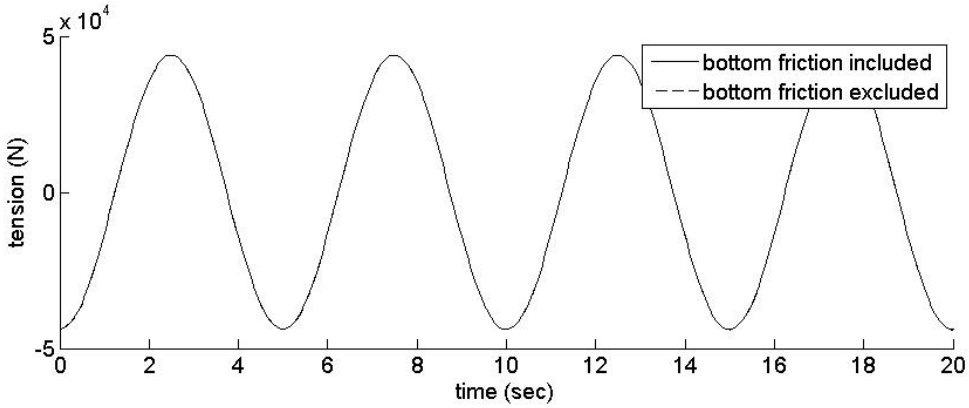

Figure 55 Tension in sway direction at fairlead under the excitation1. Result from CABLE3D for case 3.

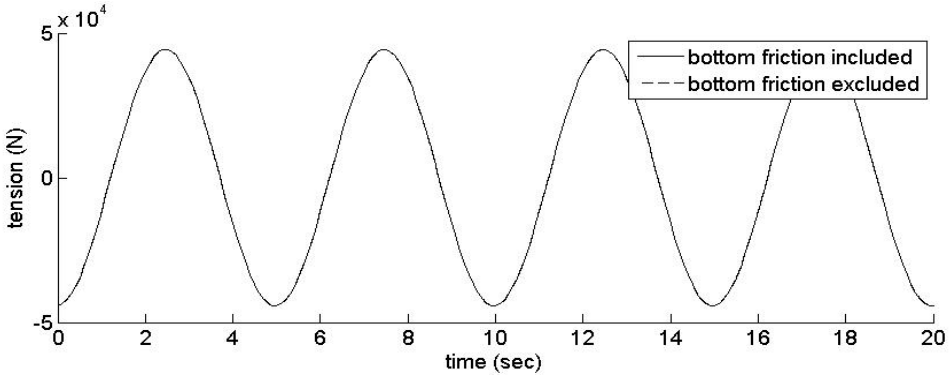

Figure 56 Tension in sway direction at fairlead under the excitation 1. Result from Orcaflex for case 3.

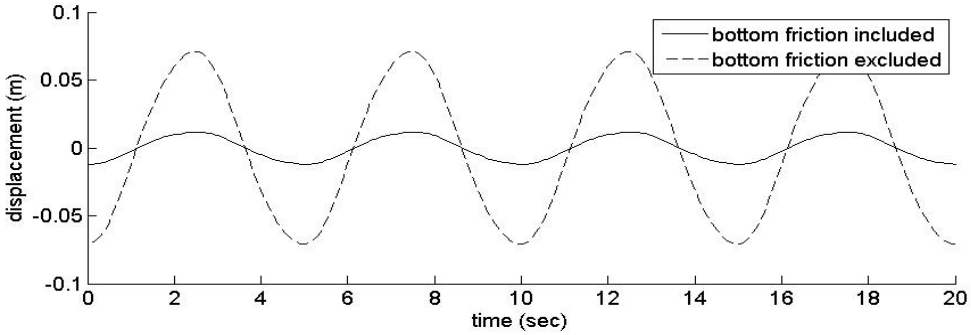

Figure 57 Displacement of the first node after TDP in sway direction under the excitation1. Result from CABLE3D for case 3.

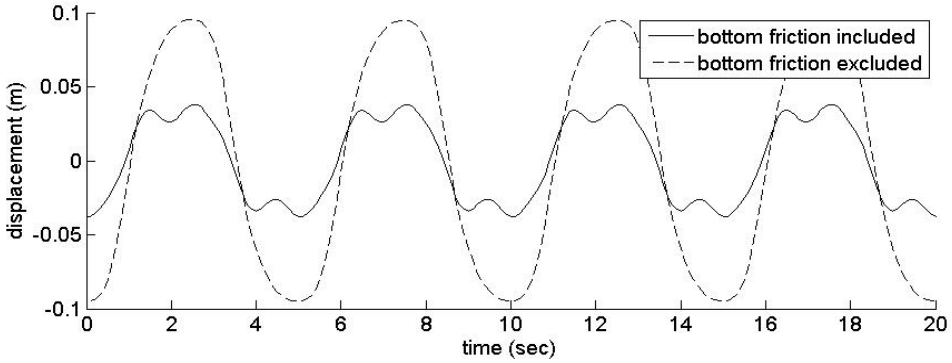

Figure 58 Displacement of the first node after TDP in sway direction under the excitation1. Result from Orcaflex for case 3.

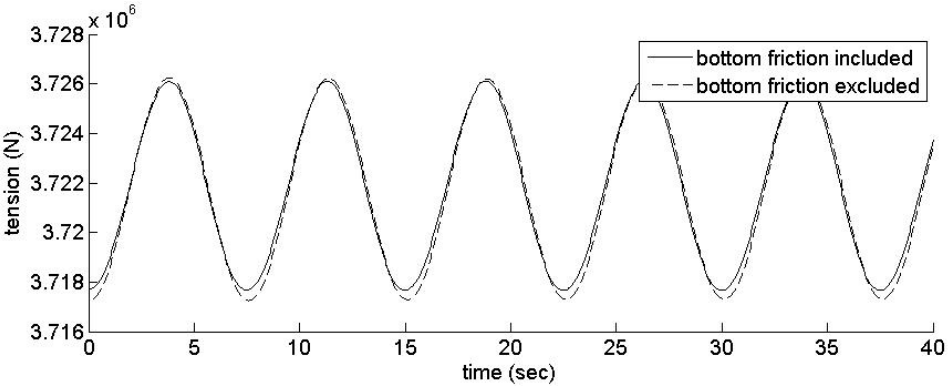

Figure 59 Total tension at fairlead under the excitation 2. Result from CABLE3D for case 3.

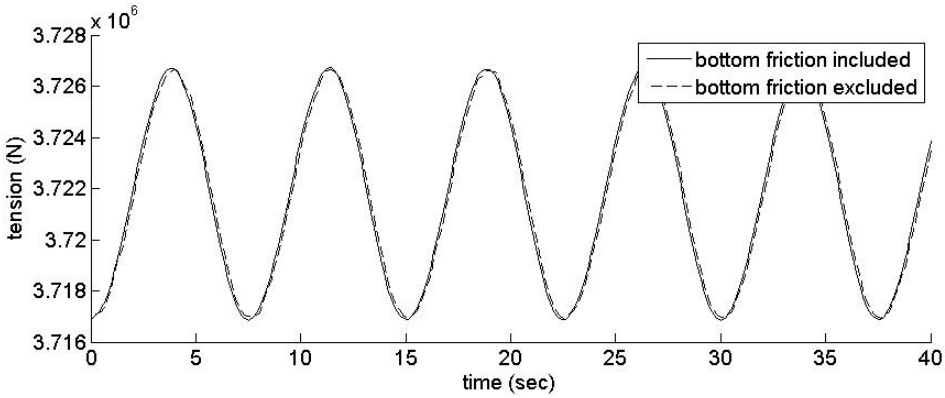

Figure 60 Total tension at fairlead under the excitation2. Result from Orcaflex for case 3.

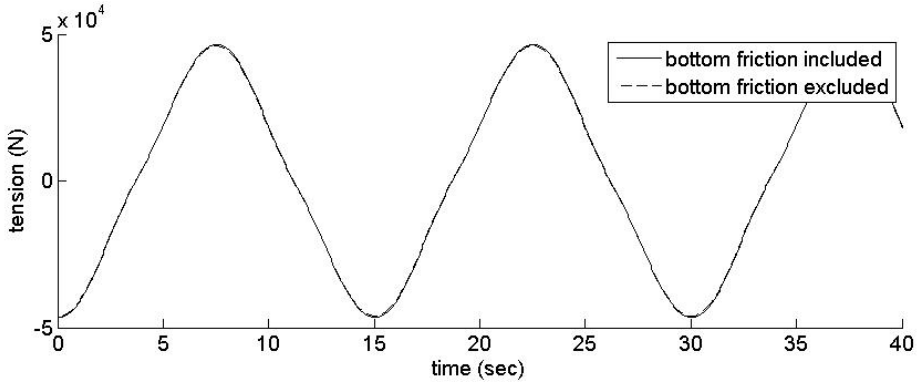

Figure 61 Tension in sway direction at fairlead under the excitation2. Result from CABLE3D for case 3.

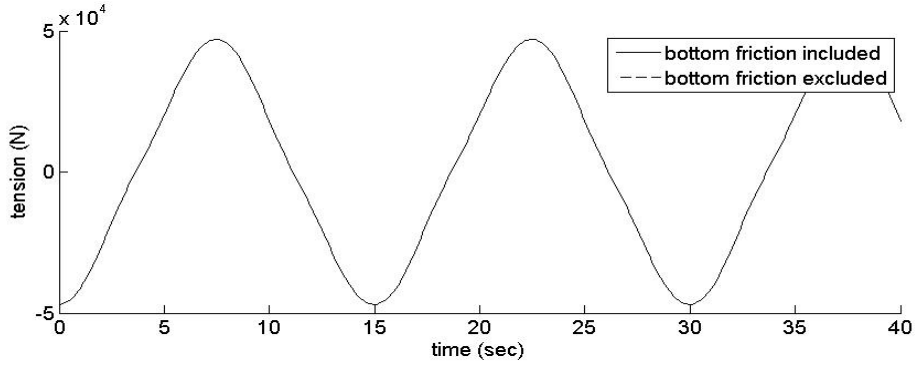

Figure 62 Tension in sway direction at fairlead under the excitation2. Result from Orcaflex for case 3.

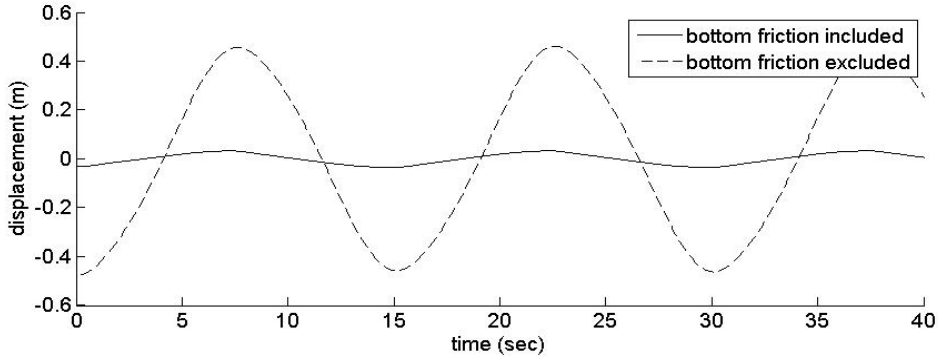

Figure 63 Displacement of the first node after TDP in sway direction under the excitation 2. Result from CABLE3D for case 3.

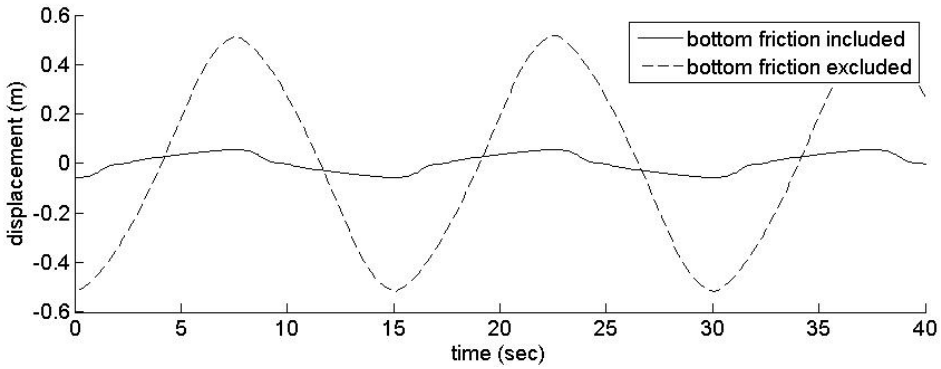

Figure 64 Displacement of the first node after TDP in sway direction under the excitation2. Result from Orcaflex for case 3.

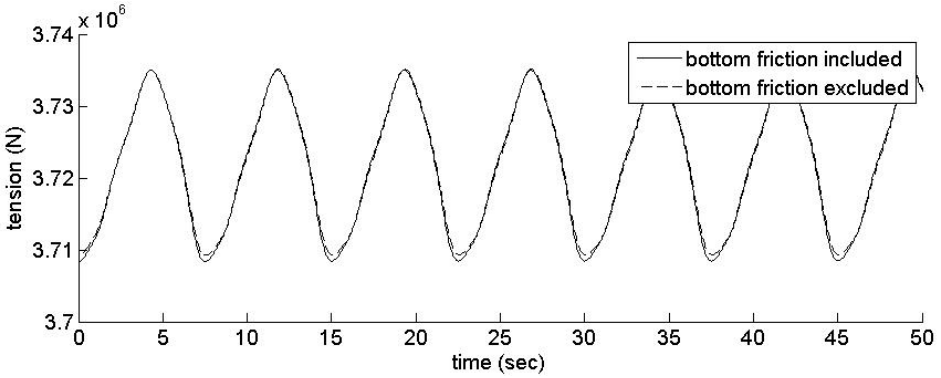

Figure 65 Total tension at fairlead under the excitation3. Result from CABLE3D for case 3.

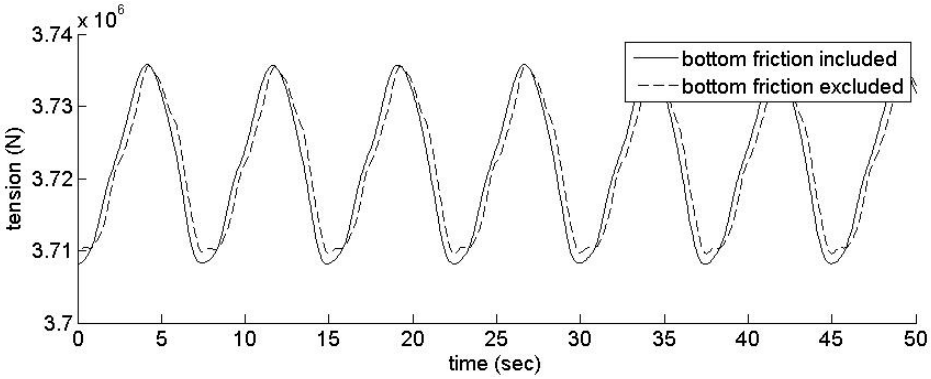

Figure 66 Total tension at fairlead under the excitation3. Result from Orcaflex for case 3.

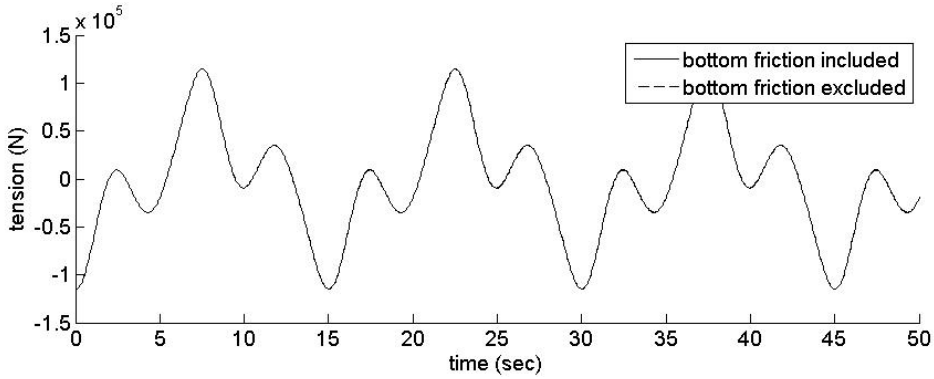

Figure 67 Tension in sway direction at fairlead under the excitation3. Result from CABLE3D for case 3.

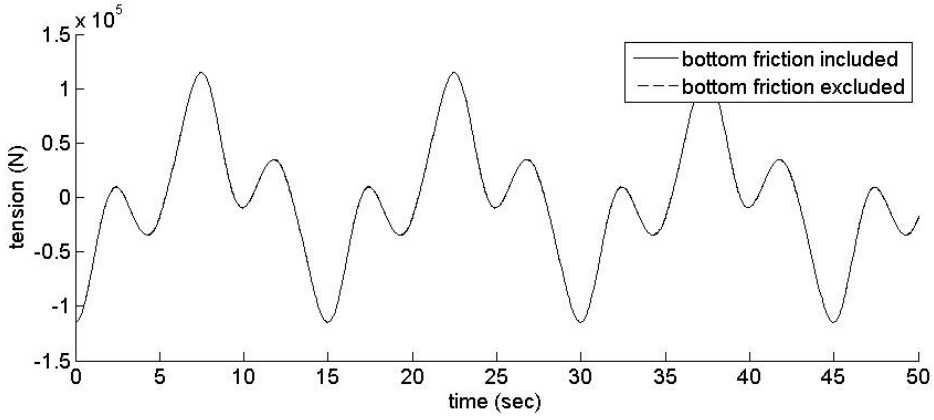

Figure 68 Tension in sway direction at fairlead under the excitation3. Result from Orcaflex for case 3.

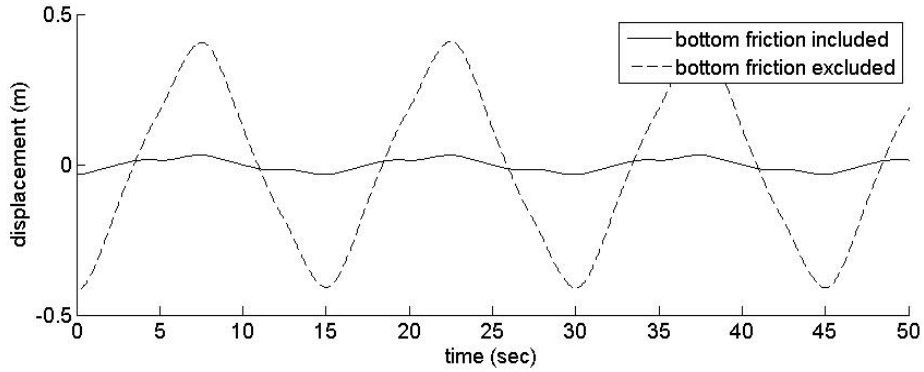

Figure 69 Displacement of the first node after TDP in sway direction under the excitation3. Result from CABLE3D for case 3.

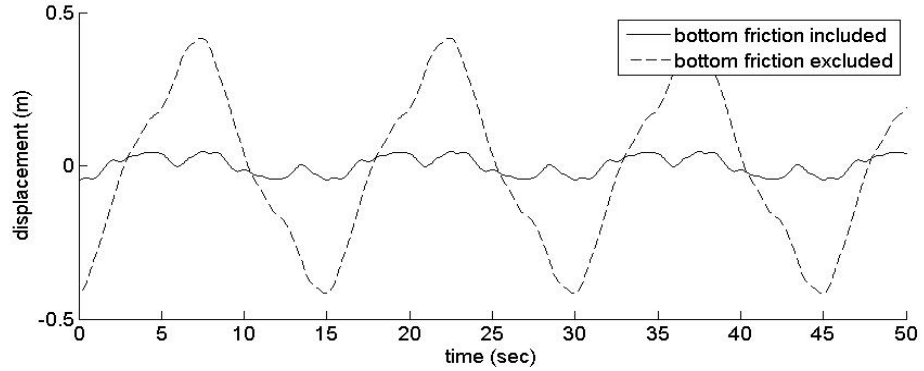

Figure 70 Displacement of the first node after TDP in sway direction under the excitation3. Result from Orcaflex for case 3.

In the case where excitation 2 is imposed, the results of the tension in the sway direction and the node motion are in satisfactory agreement between CABLE3D and Orcaflex, as shown in Figures from 61 to 64, except for the node motion with bottom friction considered. From the solid line in Figures 63 and 64, CABLE3D gives smoothly prediction of motion while Orcaflex predicts the node motion with some roughness. It can be seen from Figures 59 and 60 that, considering the bottom friction, CABLE3D predicts a little lower peaks and higher troughs of the total tension at the fairlead while Orcaflex predicts slightly lower trough values. But the differences are small enough to be ignored.

Finally, under the superposition excitation (excitation 3), the friction effect does not lead to much difference on the total tension and its component, as Figures from 65 to 68 indicate. Nevertheless, the motion about the sliding nodes after the TDP, predicted by Orcaflex in Figure 70, has high-frequency energy when ignoring the friction effect. Physically, little of the high-frequency energy is able to reach down to the mooring line on the seafloor. Therefore, the response of high-frequency is supposed to be very small, even though we cannot calculate it quantitatively. But it is obvious that, in Figure 70, the high-frequency response with bottom friction considered is due to the friction model Orcaflex uses.

4.2.4 Excitations in combination of sway and heave or sway and surge directions

As the results shown above, it is obvious that the mooring line in shallow water depth is more sensitive to the impact of the bottom friction. Therefore, another two superposed excitations are imposed at the fairlead to further reveal the bottom friction effect. These two excitations are described below:

Superposed excitation 1: a harmonic excitation with a period of 7s and amplitude of 1.5m in heave direction superposed with a harmonic excitation with a period of 5s and an amplitude of 5m in sway direction.

Superposed excitation 2: a harmonic excitation with a period of 147s and amplitude of 5m in surge direction superposed with a harmonic excitation with a period of 5s and an amplitude of 5m in sway direction.

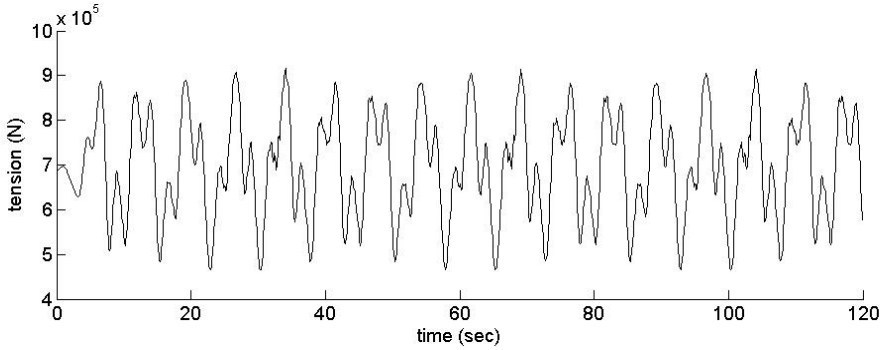

Figure 71 Total tension at fairlead under the superposed excitation 1. Result from Orcaflex with bottom friction excluded.

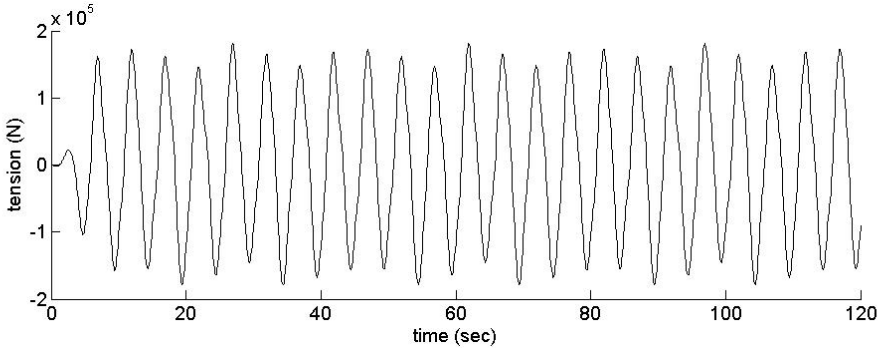

Figure 72 Tension component in sway direction at fairlead under the superposed excitation 1. Result from Ocaflex with bottom friction excluded.

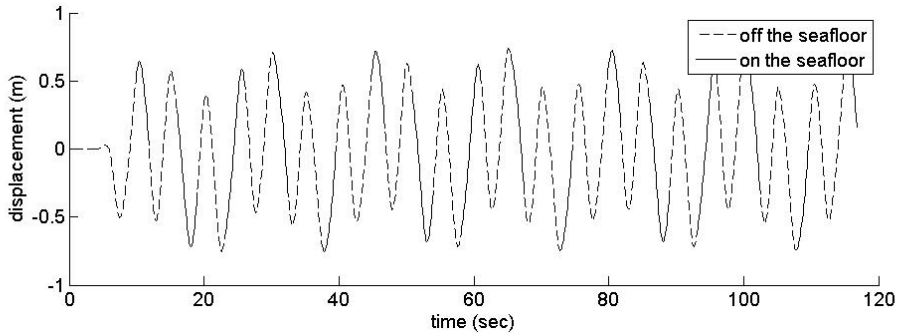

Figure 73 Displacement of Node 35 in sway direction under superposed excitation 1. Result from Orcaflex with bottom friction excluded.

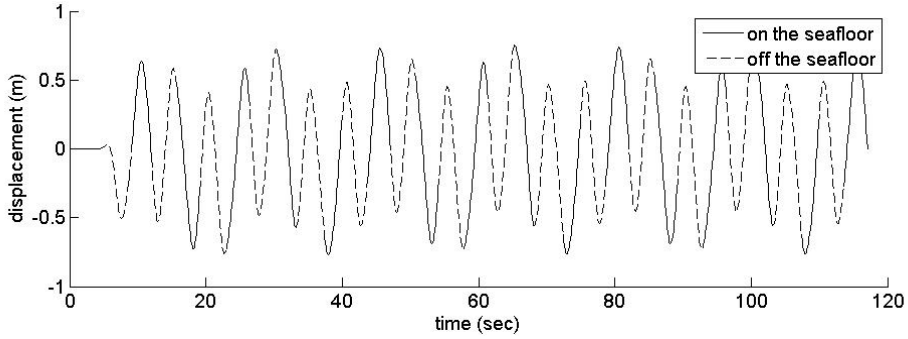

Figure 74 Displacement of Node 37 in sway direction under superposed excitation 1. Result from Orcaflex with bottom friction excluded

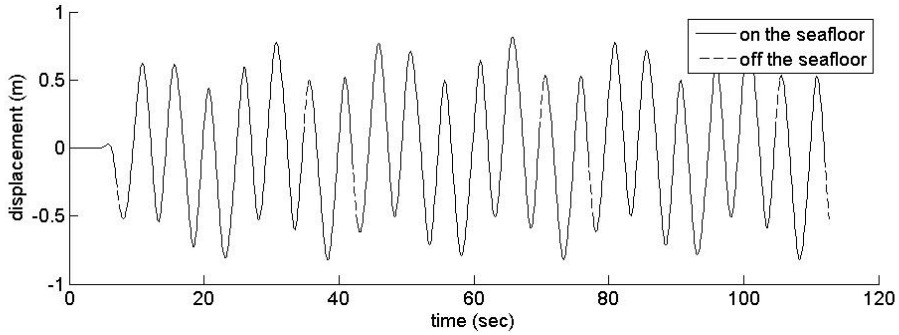

Figure 75 Displacement of Node 44 in sway direction under superposed excitation 1. Result from Orcaflex with bottom friction excluded.

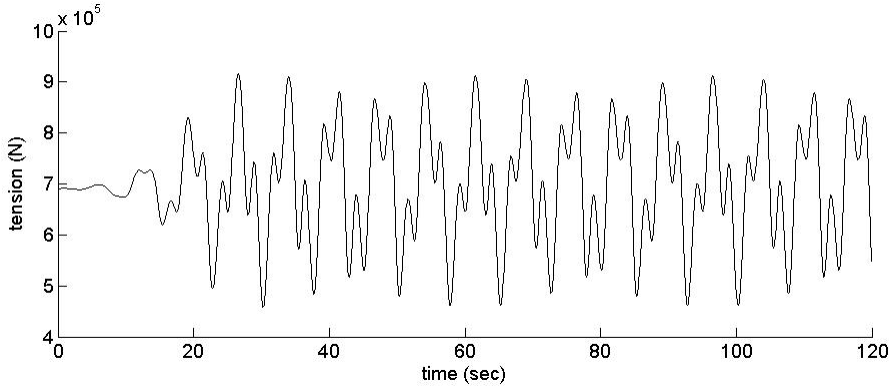

Figure 76 Total tension at fairlead under the superposed excitation 1. Result from CABLE3D with bottom friction excluded.

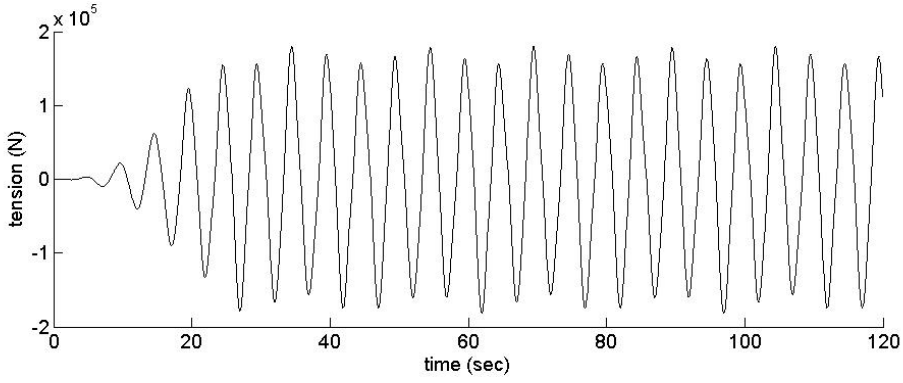

Figure 77 Tension component in sway direction at fairlead under the superposed excitation 1. Result from CABLE3D with bottom friction excluded.

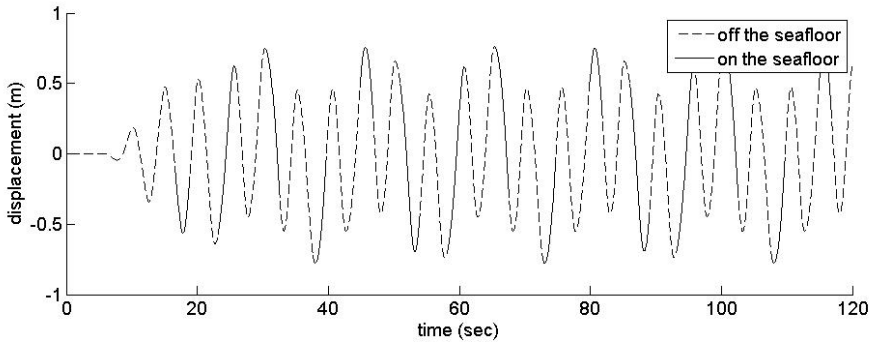

Figure 78 Displacement of Node 37 in sway direction under superposed excitation 1. Result from CABLE3D with bottom friction excluded.

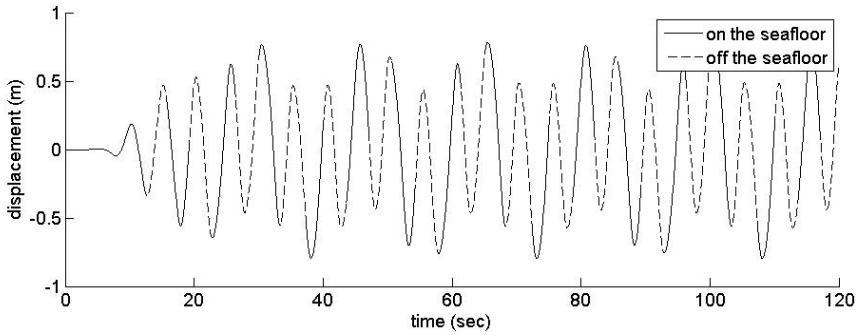

Figure 79 Displacement of Node 39 in sway direction under superposed excitation 1. Result from CABLE3D with bottom friction excluded.

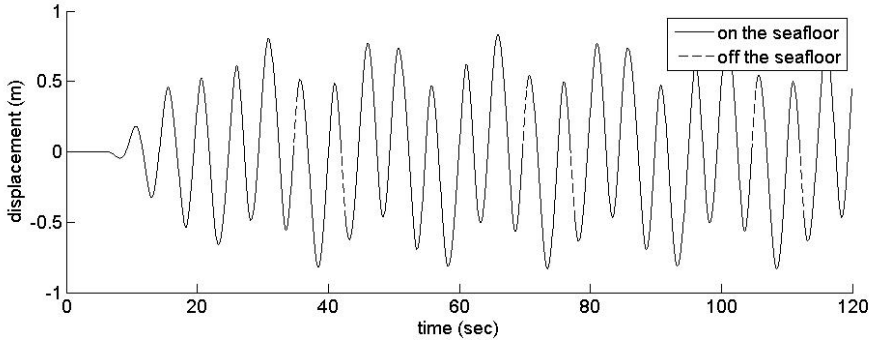

Figure 80 Displacement of Node 46 in sway direction under superposed excitation 1. Result from CABLE3D with bottom friction excluded.

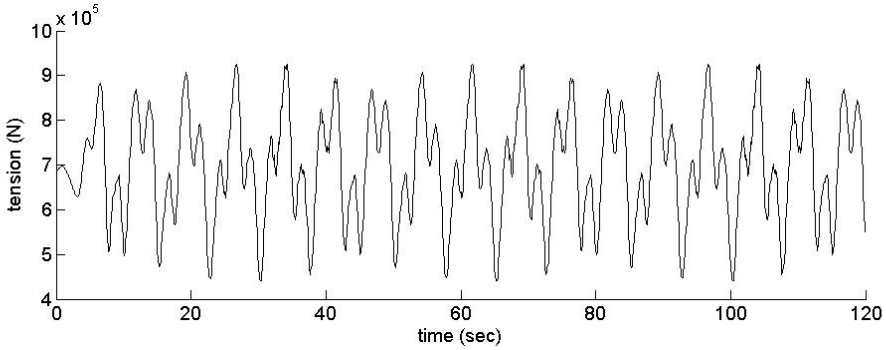

Figure 81 Total tension at fairlead under the superposed excitation 1. Result from Orcaflex with bottom friction included.

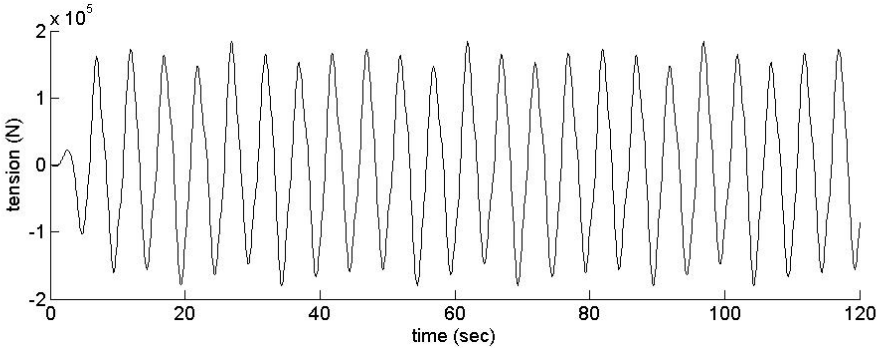

Figure 82 Tension component in sway direction at fairlead under the superposed excitation 1. Result from Ocaflex with bottom friction included.

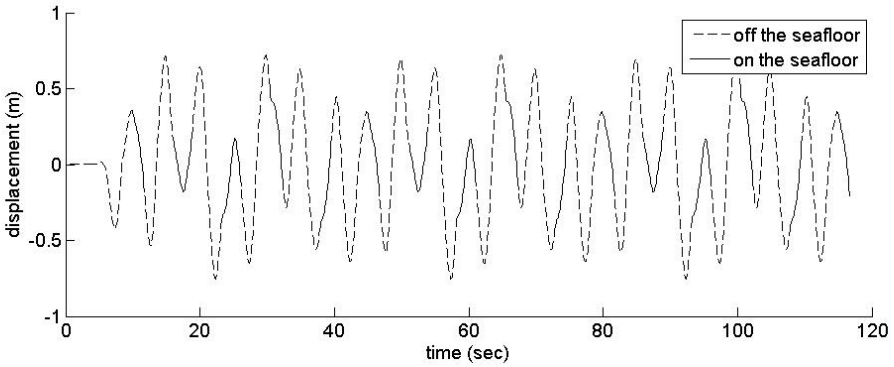

Figure 83 Displacement of Node 35 in sway direction under superposed excitation 1. Result from Orcaflex with bottom friction included.

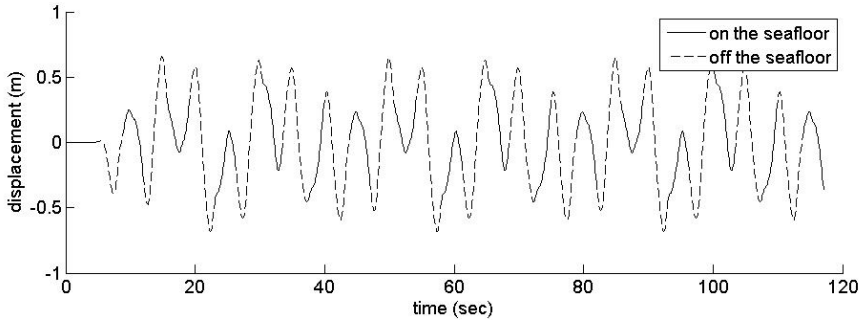

Figure 84 Displacement of Node 37 in sway direction under superposed excitation 1. Result from Orcaflex with bottom friction included.

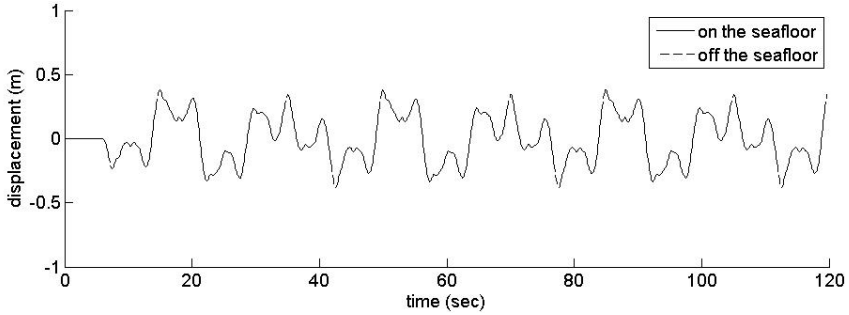

Figure 85 Displacement of Node 44 in sway direction under superposed excitation 1. Result from Orcaflex with bottom friction included.

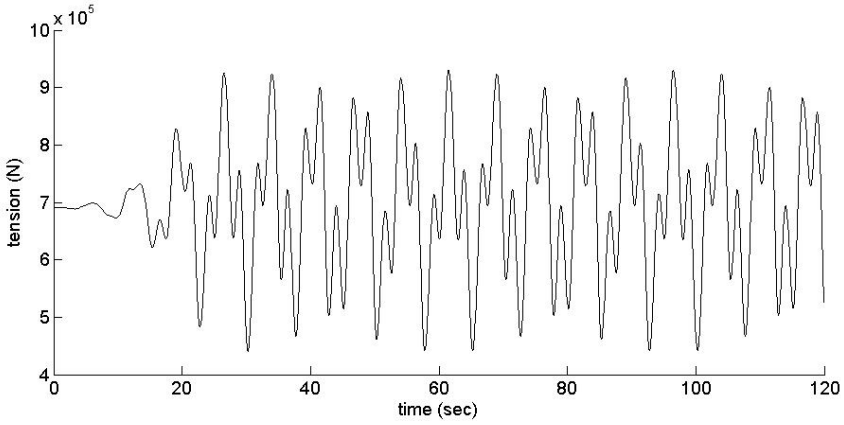

Figure 86 Total tension at fairlead under the superposed excitation 1. Result from CABLE3D with bottom friction included.

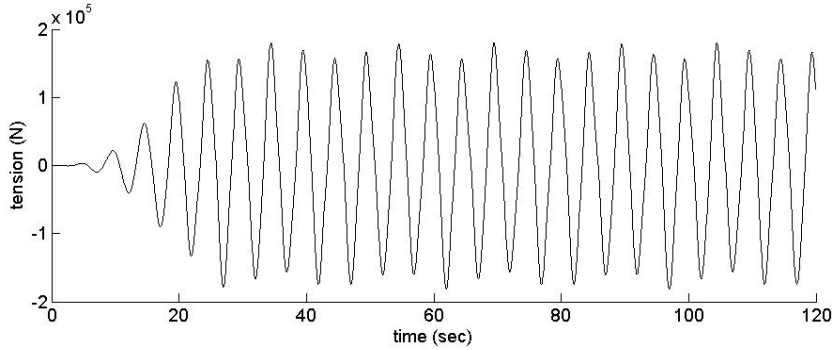

Figure 87 Tension component in sway direction at fairlead under the superposed excitation 1. Result from CABLE3D with bottom friction included.

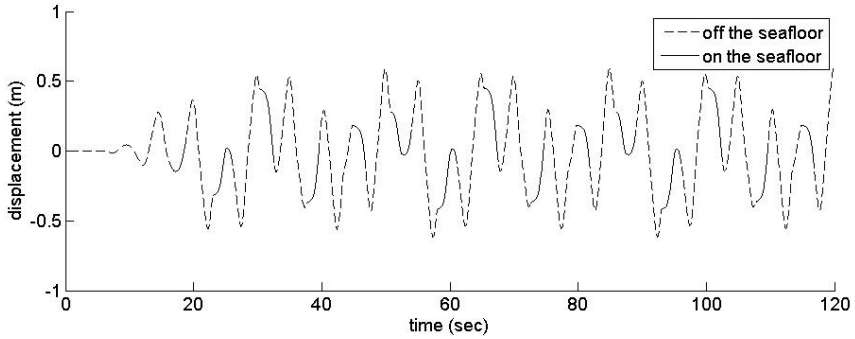

Figure 88 Displacement of Node 37 in sway direction under superposed excitation 1. Result from CABLE3D with bottom friction included.

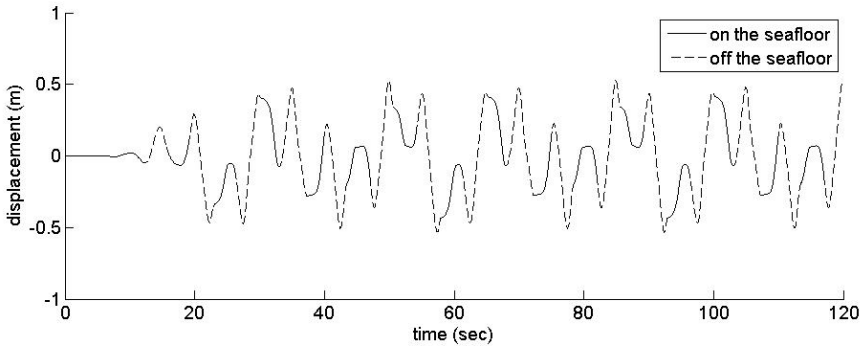

Figure 89 Displacement of Node 39 in sway direction under superposed excitation 1. Result from CABLE3D with bottom friction included.

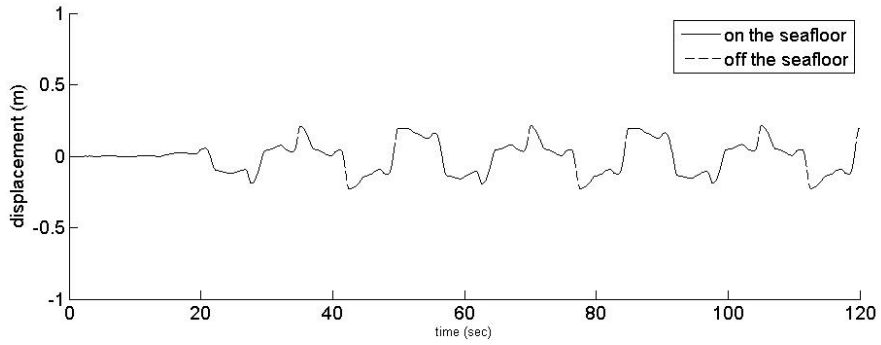

Figure 90 Displacement of Node 46 in sway direction under superposed excitation 1. Result from CABLE3D with bottom friction included.

The motion of several nodes in the neighborhood of the TDP at the equilibrium position will be discussed because the instantaneous TDP may move significantly along the mooring line following the motion in heave or surge direction at the fairlead. Furthermore, with the same element division, the Orcaflex locates the TDP between Node 36 and Node 37, while CABLE3D predicts that the TDP is between the Node 38 and the Node 39. The distance between the neighboring nodes near the TDP is 1.5m. To better compare the related results from Orcaflex and CABLE3D, the node with respect to its TDP in CABLE3D is compared with the corresponding node in Orcaflex by shifting two elements. For example, Node 38 in CABLE3D is compared with Node 36 in Orcaflex. Besides, it is noted that a 8s ramp stage is used in Orcaflex and a 30s ramp stage in CABLE3D, which are included in all the plots.

After considering the bottom friction effect, as indicated in Figures 81, 82, 86 and 87, the maximum value of the total tension increased about 1.6% and the minimum value of the total tension decreased about 3.6%, while the peak and trough values of the force component in sway direction remain almost the same, compared with the Figures 71, 72, 76 and 77. As shown in Figures 73 to 75 and 78 to 80, when the bottom friction is considered, the motion amplitude of the node is greatly reduced when the node is sliding on the ground in the sway direction. That is, the motion of sliding is significantly constrained by the bottom friction. By comparing the equivalent results from Orcaflex and CABLE3D, the motion amplitude predicted by CABLE3D is smaller than that from the Orcaflex, which is consistent with the observation made in the previous cases. However, the patterns of the curves are quite similar.

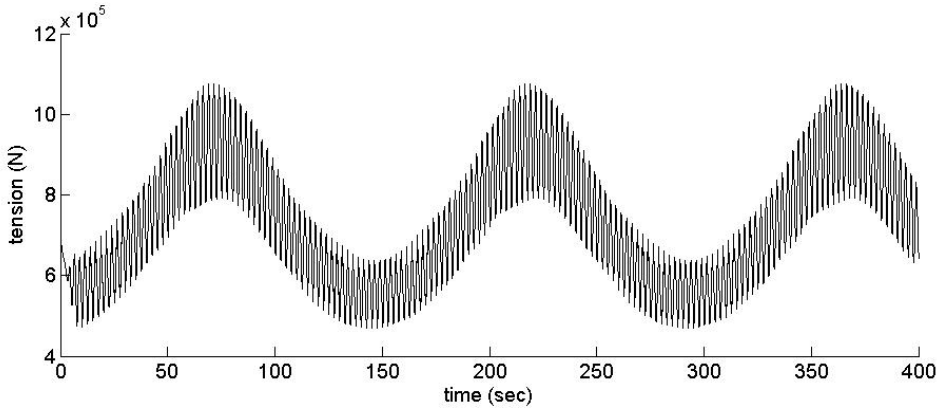

Figure 91 Total tension at fairlead under the superposed excitation 2. Result from Orcaflex with bottom friction excluded.

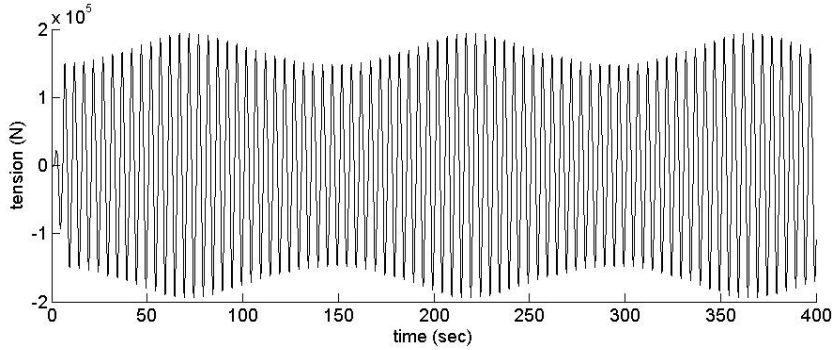

Figure 92 Tension component in sway direction at fairlead under the superposed excitation 2. Result from Ocaflex with bottom friction excluded.

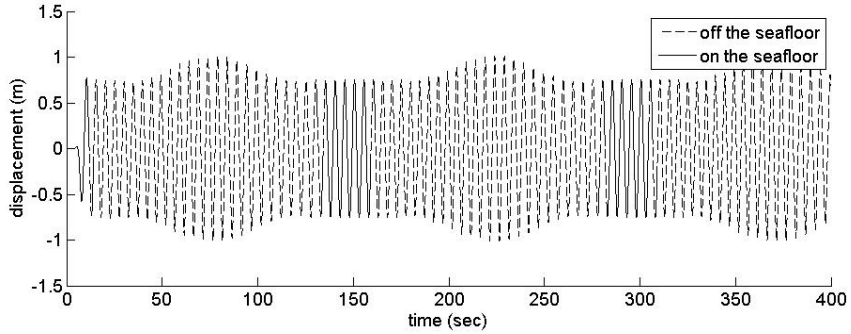

Figure 93 Displacement of Node 26 in sway direction under superposed excitation 2. Result from Orcaflex with bottom friction excluded.

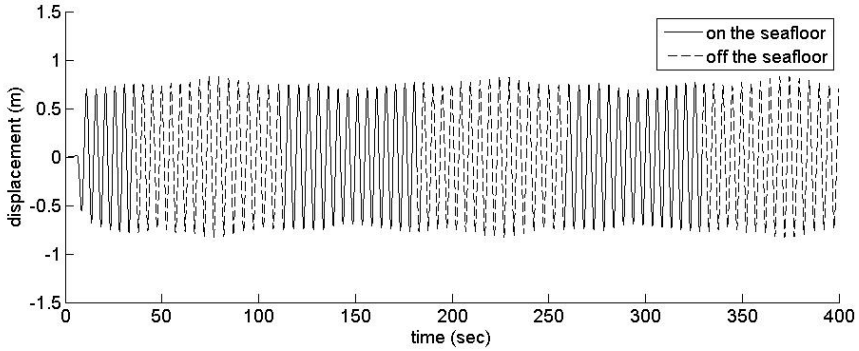

Figure 94 Displacement of Node 37 in sway direction under superposed excitation 2. Result from Orcaflex with bottom friction excluded.

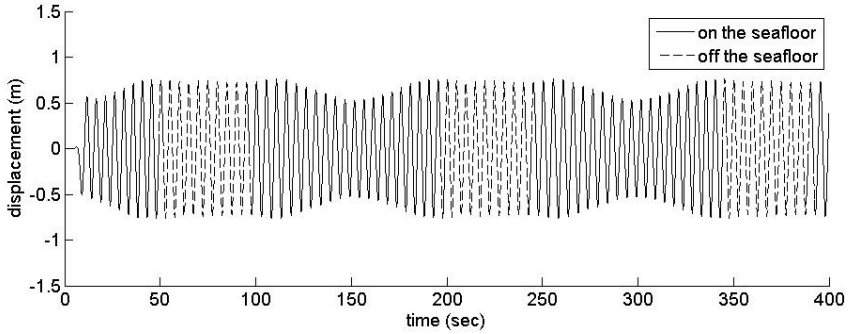

Figure 95 Displacement of Node 48 in sway direction under superposed excitation 2. Result from Orcaflex with bottom friction excluded.

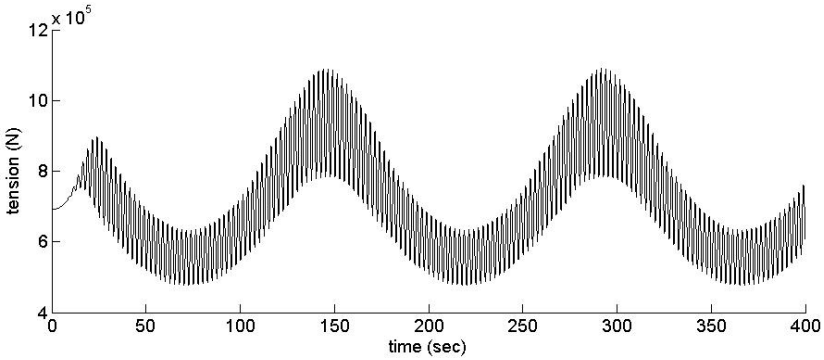

Figure 96 Total tension at fairlead under the superposed excitation 2. Result from CABLE3D with bottom friction excluded.

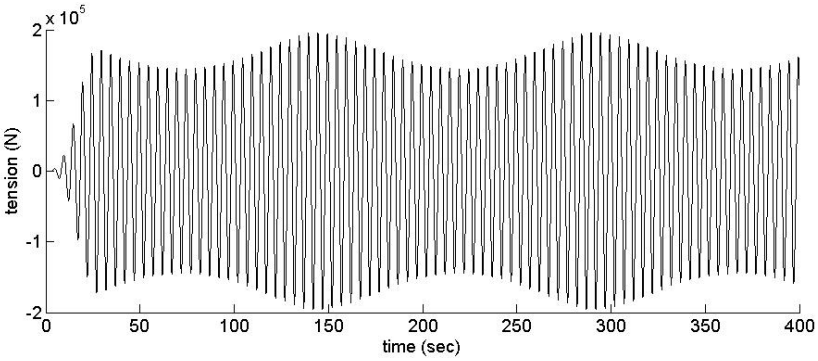

Figure 97 Tension component in sway direction at fairlead under the superposed excitation 2. Result from CABLE3D with bottom friction excluded.

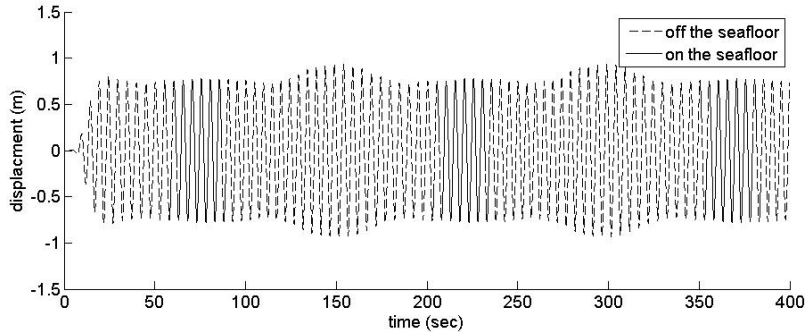

Figure 98 Displacement of Node 28 in sway direction under superposed excitation 2. Result from CABLE3D with bottom friction excluded.

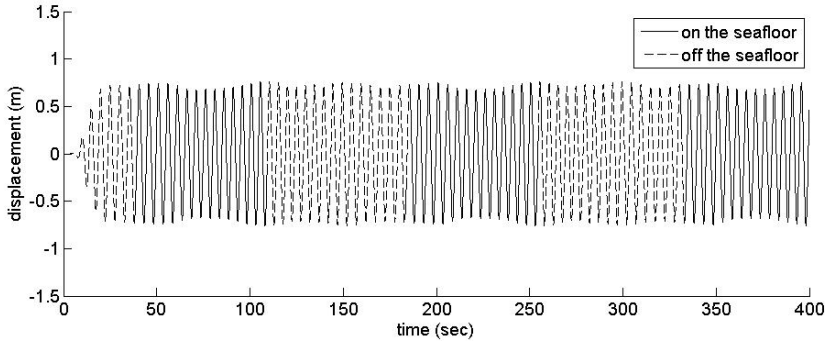

Figure 99 Displacement of Node 39 in sway direction under superposed excitation 2. Result from CABLE3D with bottom friction excluded.

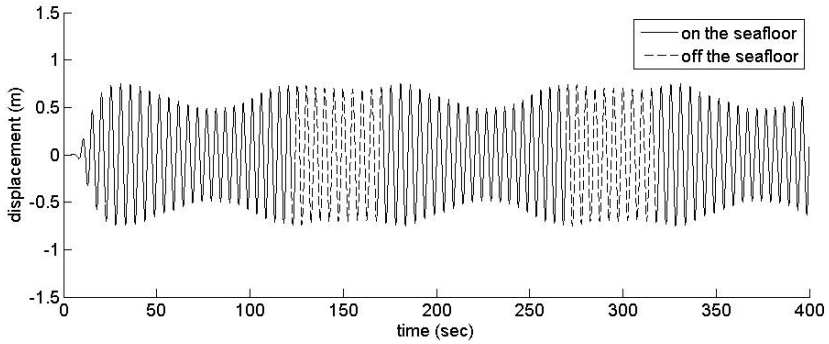

Figure 100 Displacement of Node 50 in sway direction under superposed excitation 2. Result from CABLE3D with bottom friction excluded.

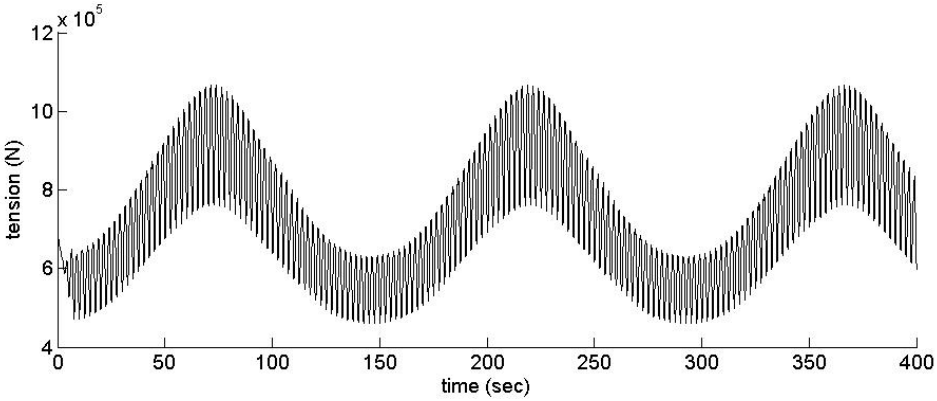

Figure 101 Total tension at fairlead under the superposed excitation 2. Result from Orcaflex with bottom friction included.

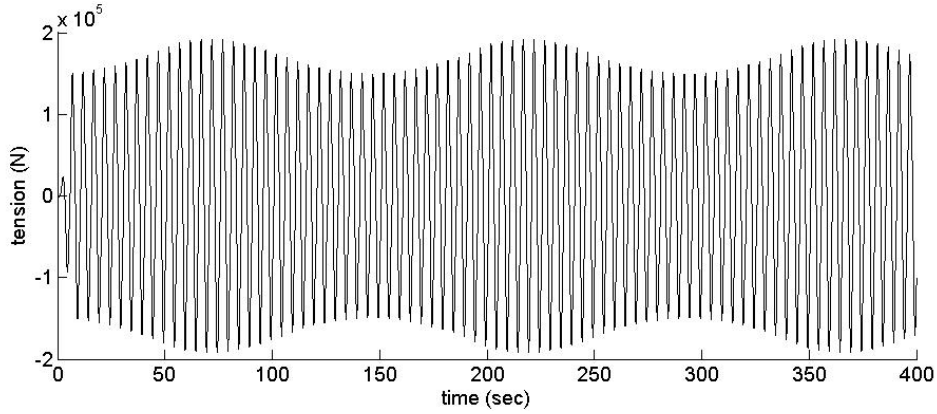

Figure 102 Tension component in sway direction at fairlead under the superposed excitation 2. Result from Ocaflex with bottom friction included.

With the superposed excitation 2 imposed at the fairlead, as shown in Figures 96 and 106, the peak value decreased about 1.4% and the trough value increased about 2.7%, based on the result from CABLE3D when the bottom friction is considered. Orcaflex predicts that the maximum and minimum values of the total force decreased about 1% and 2% respectively. While, the bottom friction effect leads to only less than 1% differece at the peaks of the force component in sway direction. However, Figures 93 to 95 and 103 to 105, show that the motion of the node is constrained when the node is in contact with the seafloor, which indicates the bottom friction plays the role. CABE3D also show that the motion is constrained when the bottom friction is imposed, by comparing Figures 98 to 100 with Figures 108 to 110.

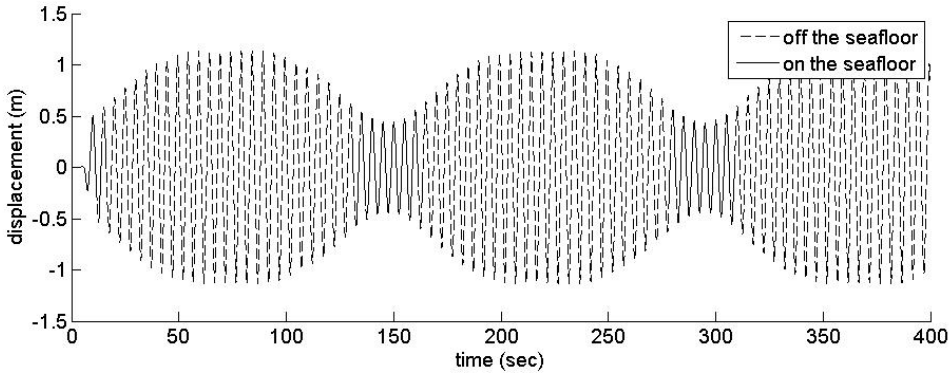

Figure 103 Displacement of Node 26 in sway direction under superposed excitation 2. Result from Orcaflex with bottom friction included.

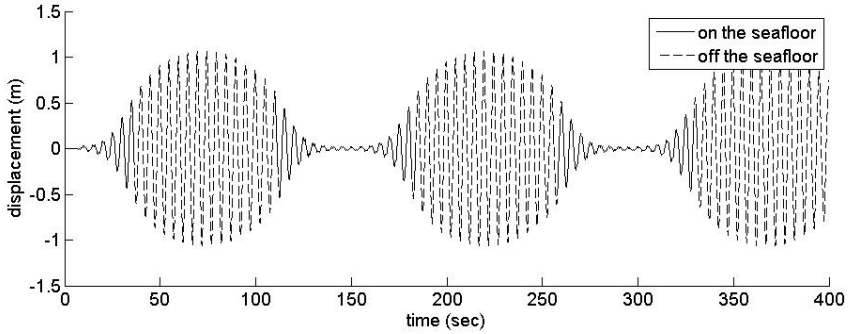

Figure 104 Displacement of Node 37 in sway direction under superposed excitation 2. Result from Orcaflex with bottom friction included.

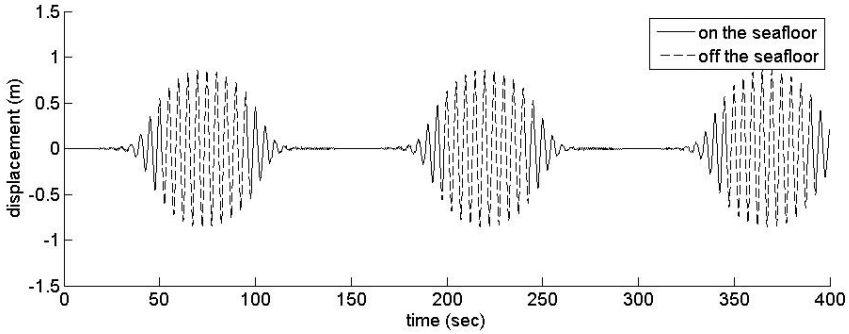

Figure 105 Displacement of Node 48 in sway direction under superposed excitation 2. Result from Orcaflex with bottom friction included.

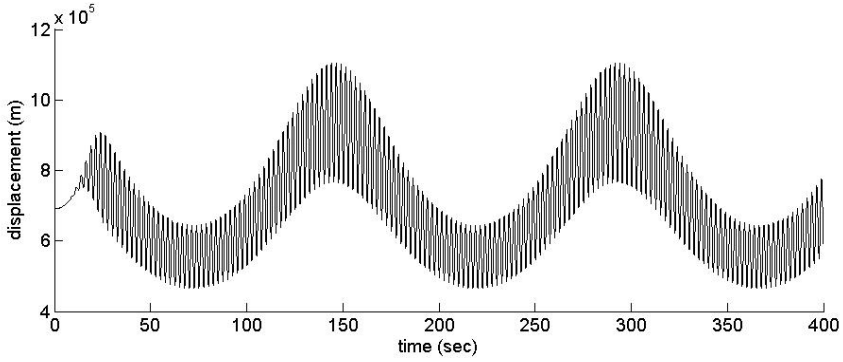

Figure 106 Total tension at fairlead under the superposed excitation 2. Result from CABLE3D with bottom friction included.

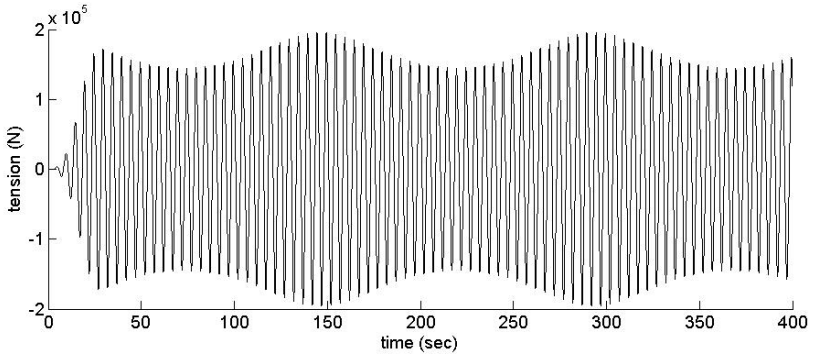

Figure 107 Tension component in sway direction at fairlead under the superposed excitation 2. Result from CABLE3D with bottom friction included.

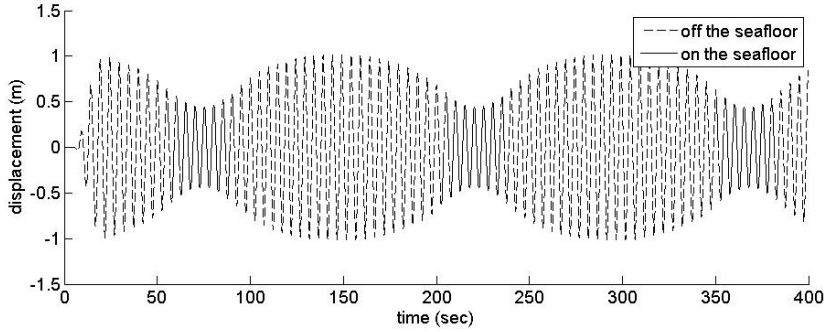

Figure 108 Displacement of Node 28 in sway direction under superposed excitation 2. Result from CABLE3D with bottom friction included.

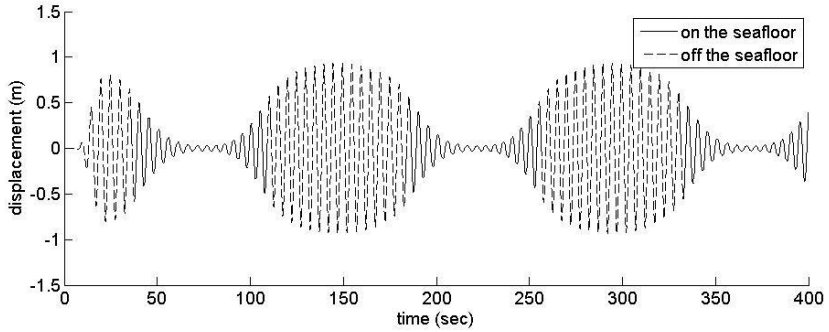

Figure 109 Displacement of Node 39 in sway direction under superposed excitation 2. Result from CABLE3D with bottom friction included.

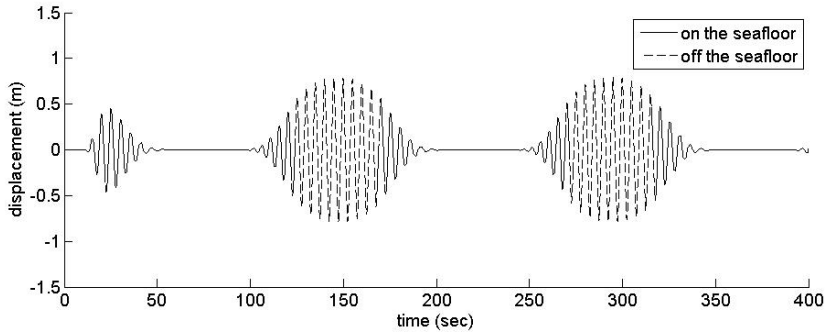

Figure 110 Displacement of Node 50 in sway direction under superposed excitation 2. Result from CABLE3D with bottom friction included.

5. CONCLUSION

In this study, the existing version of CABLE3D is extended to allow for the transverse bottom friction. A new model for determining the seafloor friction coefficient was proposed by combining two existing models. One of them depends on the transverse displacement sliding on the seafloor and the other depends on the velocity. From the comparison among the results from analytic solution and numerical simulation from CABLE3D and Orcaflex, we may draw the conclusion that the extended version CABLE3D is capable of simulating the transverse friction effectively. Also, from the results on dynamic analysis, the main conclusions to be drawn are:

1. The bottom friction produces greater impact on the mooring lines deployed in shallow depth water.
2. The bottom friction may not necessarily increase the dynamic force or maximum value of the total tension at the fairlead.
3. The bottom friction has limited impact on tension component in sway direction at the fairlead.
4. For the portion of a mooring line sliding on the seafloor, its sway amplitude is reduced significantly when we take the friction effect into account.

Besides, with the application of the friction model proposed in this study, the results from CABLE3D show the improvements in comparison with those of Orcaflex. Namely, CABLE3D predicts very smooth motion of the node right after the TDP. CABLE3D can also better simulate the sticking effect of the mooring line, that is, the static friction is properly imposed on the mooring line. Additionally, when the mooring line is sliding, its motion is fuller constraint under the new model.

In summary, the existing version of CABLE3D allows for the bottom friction in the transverse direction when the portion of a mooring line slides on the seafloor. The model is robust, easy to converge and likely performs better than Orcaflex.

REFERENCES

Brown, D.T., Lyons, G. J., and Lin, H. M., 1997, Large-scale testing for mooring line hydrodynamic contributions at combined wave and drift frequencies. In: Proceedings of the Eleventh BOSS (Belgian Organic Synthesis Symposium) Conference, Ghent, Belgium.

Chen, X., 2002. Studies on Dynamic Interaction between Deep-water Floating Structure and Their Mooring/Tendon Systems. Texas A&M University. Doctor of Philosophy. College Station, US.

Chen, X., Zhang, J., Johnson, P., Irani, M., 2001. Dynamic analysis of mooring lines with inserted springs. Applied Ocean Research 23, 277-284.

Chung, J., 1993. A time integration algorithm for structural dynamics with improved numerical dissipation: the generalized-α method. Journal of Applied Mechanics 60, 2-371.

Garrett, D.L., 1982. Dynamic analysis of slender rods. Journal of Energy Resources Technology, ASME Transaction 104, 302-307.

Inoue, Y., Surendran, S., 1994. Dynamics of the interaction of mooring lines with the seabed. In: Proceedings of the Fourth International Offshore and Polar Engineering Conference, Osaka, Japan.

Jonkman, J.M, 2009. Definition of the floating system for phase IV of OC3. National Renewable Energy Laboratory, Golden, CO.

Leonard, J.W., Nath, J.H., 1981. Comparison of finite element and lumped parameter method for oceanic cables. Engineering Structures 3(3), 153-167.

Lindahl, L., Sjöberg, A., 1983. Dynamic analysis of mooring cables. In: Proceeding of the Second International Symposium on Ocean Engineering and Ship and Handling, Gothenburg, Sweden.

Liu, Y., Bergdahl, L., 1997. Influence of current and seabed friction on mooring cable response: comparison between time-domain and frequency-domain analysis. Engineering Structures 19, 945-953.

Ma, W., Webster, W.C., 1994. Analytical approach to cable dynamics: Theory and user manual. Sea Grant Project R/OE-26.

Nakamura, N., Koterayama, W., Kyozuka, Y., 1991. Slow drift damping due to drag forces acting on mooring lines. Ocean Engineering 18, 283-296.

Newmark, N. M., 1959. A method of computation for structural dynamics. Journal of Engineering Mechanics, ASCE, 85 (EM3) 67-94.

Teng, C.C., Wang, H.T., 1995. Mooring of surface wave following buoys in shallow water. In: Proceedings of the Fourteenth International Conference on Offshore Mechanics and Arctic Engineering, Copenhagen, Denmark.

Thomas, D.O., 1993. A Numerical Investigation of Time Integration Schemes Applied to the Dynamic Solution of Mooring Lines. The University of Newcastle upon Tyne. Doctor of Philosophy. Newcastle, UK.

Triantafyllou, M.S., Bliek, A., Shin, H., 1985. Dynamic analysis as a tool for open-sea mooring system design. SNAME Transactions, 93, 302-324.

Webster, R.L., 1975. Non-linear static and dynamic response of underwater cable structures using finite element approach. In: Proceeding of the Seventh Offshore Technology Conference, Houston, US.

Wu, S., 1999. Investigation into three mooring line-seabed interaction models for frequency-domain mooring line dynamic analysis. In: Proceedings of the Ninth International Offshore and Polar Engineering Conference, Brest, France.

Webster, W.C., 1995. Mooring induced damping. Ocean Engineering 22, 57-591.

VITA

Name: Hang Lu

Address: Zachry Department of Civil Engineering

Texas A&M University

3136 TAMU

College Station, Texas 77843-3136

USA

Email Address: serennia@tamu.edu

Education: B.E., Naval Architecture and Ocean Engineering, Wuhan University of Technology, 2006